2021-04-03

Going for Gold: Point of Care Bio-Diagnostics and Gold Nanoparticles Treating Disease

Trevor M. Godfrey
Brigham Young University

Going for Gold: Point of Care Bio-Diagnostics and

Gold Nanoparticles Treating Disease

Trevor M. Godfrey

A thesis submitted to the faculty of
Brigham Young University
in partial fulfillment of the requirements for the degree of

Master of Science

Richard Kent Watt, Chair
Pam Van Ry
David L. Kooyman

Department of Chemistry and Biochemistry

Brigham Young University

ABSTRACT

Going for Gold: Point of Care Bio-Diagnostics and
Gold Nanoparticles Treating Disease

Trevor M. Godfrey
Department of Chemistry and Biochemistry, BYU
Master of Science

Correct diagnosis of disease is essential in the effort to save and improve lives. Point of care (POC) diagnostics are *in-vitro* tests that assist in patient diagnosis and can be used at the location of patient care. POC diagnostics are easy to use and provide near-instant readouts allowing medical providers and patients to make rapid decisions about treatment. Increased access to POC testing is especially beneficial to low-income and low resource areas that cannot afford expensive lab testing. The World Health Organization (WHO) has outlined at least 113 diseases for which POC diagnostics are needed. Because of this, developing effective, efficient, and economical methods for creating new POC tests is essential. Work in section one of this thesis describes strategies by which new POC bio-diagnostics can be created. The use of oxidized cellulose as a vector for antibody immobilization was explored in several cellulose-based materials to provide quick, economical tests while still obtaining effective limits of detection when used to detect the pregnancy hormone Human Chorionic Gonadotropin (HCG) in a proof of concept study. The majority of these tests could detect as low as 100 ng/mL of HCG well below the clinical level necessary for detection at 2400 ng/mL. The use of a hand-powered syringe-based POC named the fast flow immunoassay (FFI) was tested for its ability to increase observable signal in a sandwich immunoassay by passing the sample through the test filter multiple times. 10 passes through the filter resulted in a signal approximately 17x more intense than a 1-hour dot-blot sandwich immunoassay. Both oxidized cotton and FFI systems can be used to develop new POC assays quickly and economically. Future use of these POC systems could help expand the availability of diagnostic testing to disadvantaged areas.

Gold-based drugs have been used and investigated as medications multiple times throughout history to treat various diseases such as Rheumatoid arthritis, parasitic infections, and cancer. In the last few decades, gold nanoparticles have been used as drug delivery agents and catalysts for various reactions. Recently catalytic gold nanocrystals have been characterized for their ability to treat neurodegenerative diseases. Although these results were promising, much is still unknown about their mechanism of action. Section two of this thesis investigates potential molecular pathways that gold nanocrystals could be affecting, specifically the IL-6/Jak/STAT3 inflammation pathway and the Nrf2 antioxidant pathway. The gold nanocrystals we tested did not affect these pathways at physiologically obtainable concentrations. Additional work was done to characterize protein interactome or protein corona of gold nanocrystals. Preliminary proteomic characterization of this protein corona in fetal bovine serum (FBS) identified 118 potential interactors and classified those based on function and structure. Future work will need to be done to follow up on these identifications and to determine what mechanistic implications they may have.

Keywords: POC diagnostics, oxidized cellulose, gold nanoparticles, protein corona

ACKNOWLEDGEMENTS

There are so many people who have enabled me to complete this thesis. First and foremost I want to thank my wife Victoria for motivating, encouraging, and loving me all while completing an extremely difficult degree herself. An unknowable amount of gratitude also goes to Richard Watt, who accepted me into his lab when space was tight, for showing me how fun research can truly be, and for being an example of the kind of person and scientist that I aspire to be. A big thanks also goes to my committee members David Kooyman and Pam Van Ry for all of their excellent feedback on these projects as well as their advice that has helped me be successful in graduate school. Thank you to all the members of the Watt lab especially the other graduate students for all of the hard work and good times: from western blotting to nerf guns, from lateral flow to beagles, we've been through it all. A huge thank you goes out to Roger Woolley and John Gardener, the undergraduates who have truly helped pushed these projects forward and made it a fun time as we've gone, the best of luck to both of you in your future aspirations as doctors and scientists. I also thank the Department of Chemistry and Biochemistry and all of the amazing office staff who really run the show. Finally, I'd like to thank my Father in Heaven and my Savior for allowing me the last two years of my life to learn and grow spiritually while completing this master's degree.

TABLE OF CONTENTS

LIST OF FIGURES

SECTION 1: MODIFIED BIO-DIAGNOSTIC TESTS

BACKGROUND

Before a patient can receive treatment for a disease, they first have to know that they have that disease. The process by which a patient discovers their ailment is known as diagnosis. Diagnosis is a crucial though often overlooked area of medicine. Trained professionals can diagnose patients based on descriptions of symptoms from the patient, but this means that the disease has to have symptoms and that the patient has to communicate them effectively. Diseases with few or ambiguous symptoms can be missed in this way. Another issue that arises from diagnosis by symptoms is that one symptom can often be implicated in many conditions. An online article about headaches by the Mayo Clinic details 52 possible causes of headaches ranging from dehydration to cancer.[1] Because of this complexity, it is essential to accurately measure specific molecular disease biomarkers that can assist in diagnosis; this is accomplished using *in-vitro* diagnostics or bio-diagnostics.

Bio-diagnostics are tests that look for specific molecular biomarkers to assist in the diagnosis of disease and other conditions. Worldwide, there is a great need for in-vitro diagnostics, especially in countries with low socioeconomic status. In 2018 the World Health organization published the first essential list of bio-diagnostic tests naming 113 tests necessary to advance universal health coverage, address health emergencies, and promote healthier populations.[2,3] This focus emphasizes that even if a country has access to great medicine, it will not administer it effectively or efficiently if it cannot correctly diagnose disease in individuals using bio-diagnostics.

Some commonly used bio-diagnostics techniques include qPCR and RT-PCR, enzyme-linked immunosorbent assays (ELISA's), western blotting, mass spectrometry, and

immunological-based assays. While many of these bio-diagnostics are very sensitive and accurate, they can only be run in medical laboratories with expensive equipment and technically trained personnel. Unfortunately, these laboratories are only accessible when infrastructure and funding are sufficient, which often means that rural and low-income locations will lack access to such facilities. Because of this disparity, there is a high demand for point-of-care (POC) diagnostics.

POC diagnostics are diagnostics that can be administered in any clinic or even at home with a quick return of results. POC testing decreases the amount of time to diagnosis, reduces cost, increases clinical efficiency, and increases patients' ability to participate in their treatment.[4,5] POC diagnostics need to provide quick and non-complicated results, making it essential that these tests have a simple readout without needing advanced equipment to image the product. The World Health Organization outlined an ideal standard for POC testing named the ASSURED criteria: Affordable, Sensitive, Specific, User-friendly, Rapid and robust, Equipment-free, and Deliverable to end-users.[4] These criteria focus not only on accuracy and sensitivity but also on affordability and ease of use. These criteria are especially important to allow distribution and use of tests in countries that lack the infrastructure for more complicated diagnostics.

One of the essential parts of POC assays is obtaining a simple signal that can be read immediately. One common technique is to use colorimetric assays, in which a color change or an appearance of color corresponds to the diagnostic state being probed. Colorimetric tests can help avoid the use of complicated imaging apparatuses and make the tests easier to administer. One common way to add colorimetric character to a bio-diagnostic is by using nanoparticles. Due to the plasmon resonance exhibited on the surface of nanoparticles, a solution of nanoparticles can appear red, pink, green, blue, or another color depending on the nanoparticles' size and shape.[6] The most commonly used nanoparticles are gold nanoparticles because they are easy to synthesize, and

antibodies can be easily conjugated to gold surfaces both passively and actively, giving a high degree of flexibility in selecting analytes.[7]

One commonly used POC diagnostic technique that utilizes gold nanoparticles is the Lateral Flow Immunoassay (LFI). LFI's are a type of immunological sandwich assay that works by capillary action and generally consists of four parts: a sample pad, a conjugate pad, a test strip, and an absorbance pad (figure 1). A sample containing an analyte is added to the sample pad, which wicks the sample up the strip. As the analyte passes through the conjugate pad, gold nanoparticles conjugated to an antibody against the analyte bind to the analyte and are also wicked up the strip. Capillary flow continues to carry the analyte-antibody-nanoparticle complex up the test strip until they encounter another line of antibodies stuck to the strip specific to the analyte. These antibodies catch the analyte and form a sandwich (antibody-analyte-antibody-gold nanoparticle), which creates a visible line on the test strip due to the gold nanoparticles' aggregation. Also usually included on the test strip is a control line with antibodies specific against

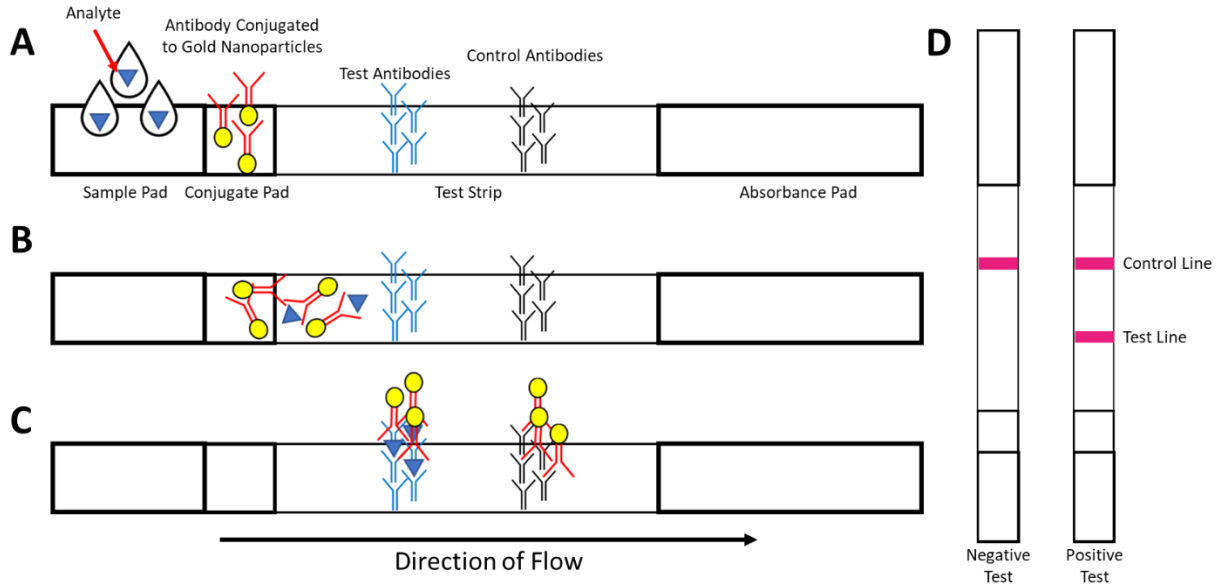

Figure 1: Lateral Flow Immunoassay Schematic. ***A:*** *Sample containing analyte is added to the sample pad.* ***B:*** *Capillary action wicks the sample up past the conjugate pad and binds to antibodies against that analyte conjugated to gold nanoparticles.* ***C:*** *The sample continues to flow up the strip and past test antibodies against the analyte and control antibodies against the conjugate antibodies.* ***D:*** *If the test is negative (contains no analyte) only the control line will appear, if the test is positive both the test and control line will appear.*

the antibodies conjugated to the gold nanoparticles. This line serves as a control to show that the test has been appropriately run (antibody-antibody-gold nanoparticle). The absorbent pad at the top of the LFI acts as a sponge, wicking up the sample and encourages capillary action.

Pregnancy tests are common LFI's that detect the presence of human chorionic gonadotropin (HCG), a protein upregulated during pregnancy, to provide evidence of a pregnancy. Another well-known LFI is the COVID19 rapid antigen test. Both pregnancy and COVID19 LFI's have similar readouts: a single line indicates that the test has run correctly but that the result is negative, two lines indicate a positive result, no lines or no control line means that the test has not run correctly and needs to be redone.

Lateral flow immunoassays are extremely useful POC diagnostics that can be adapted to test for almost any analyte as long as antibodies against the analyte exist. Even so, the design and development process can make the production of new LFI's time-intensive. Good antibody pairs have to be found, conjugate pad composition has to be optimized, and specialized buffers for analyte extraction may need to be tested. All of these factors can slow the rate at which a new LFI is brought from the lab bench to the user's hands which can be very detrimental to communities when needed quickly. These limitations were evident during the beginning of the COVID19 pandemic. It took developers several months to develop the COVID19 Rapid antigen LFI tests, allowing the disease to spread for those extra months.[8] Quicker development of LFI's could help reduce future pandemics' effects.[9]

While LFI's are simple to use, the complexities in development mentioned above make it difficult for low-funded laboratories to make new LFI's. While this may not be a problem in the United States, developing countries should not have to wait for a benevolent 1st world nation to meet their diagnostic needs. One goal of this research project is to develop methods to make new

POC assays for measuring biomarkers quickly and easily with little equipment so developing countries can meet their own bio-diagnostic needs.

In addition to the limitations mentioned above, LFI's do not work with every type of analyte. Analytes not in an aqueous solution have to be solubilized before an LFI can be used. If an analyte is not soluble in an aqueous fluid, then complicated extraction/solubilization buffers will be needed. Additionally, some biological vectors are challenging to use in LFI formats due to their high viscosity, impeding capillary flow. Saliva is an example of a biological vector that is difficult to use in an LFI, mainly because of its high mucus content.

These factors show that while LFI's are fantastic point-of-care assays, they are not ideal in every situation. New POC bio-diagnostics are needed to provide diagnosis in areas that LFI's cannot. The purpose of this section of my thesis is to outline potential materials and strategies that can be used in future POC tests to accomplish this.

CHAPTER 1: Oxidized Cellulose in Point of Care Diagnostics

Introduction

Traditionally, the test strip on the LFI strips is made out of nitrocellulose, which binds strongly to proteins with hydrophobic and electrostatic interactions. While nitrocellulose works well in LFI applications, it has several physical limitations, such as becoming brittle when dry, moderate absorbency, and low flexibility. Additionally, if the purchase of nitrocellulose is not financially feasible, the preparation of nitrocellulose in a low-income setting is dangerous because concentrated nitric acid and sulfuric acid are required during the manufacturing process and because nitrocellulose is highly flammable. The poor absorbency of nitrocellulose also slows diagnostic runtime and necessitates the use of absorbent pads. These factors make nitrocellulose challenging to use in some styles of bio-diagnostics. Because of these issues, we decided to explore another protein-binding material that can easily be made in a lab with minimal resources as an alternative to nitrocellulose: oxidized cellulose.

Cellulose is a polysaccharide made from β(1-4) linked D-glucose chains. When placed with a potent oxidizing agent (such as potassium periodate), the glucose subunits open up between carbon-2 and carbon-3, forming two aldehydes on either end (figure 2).[10,11] Proteins can be added

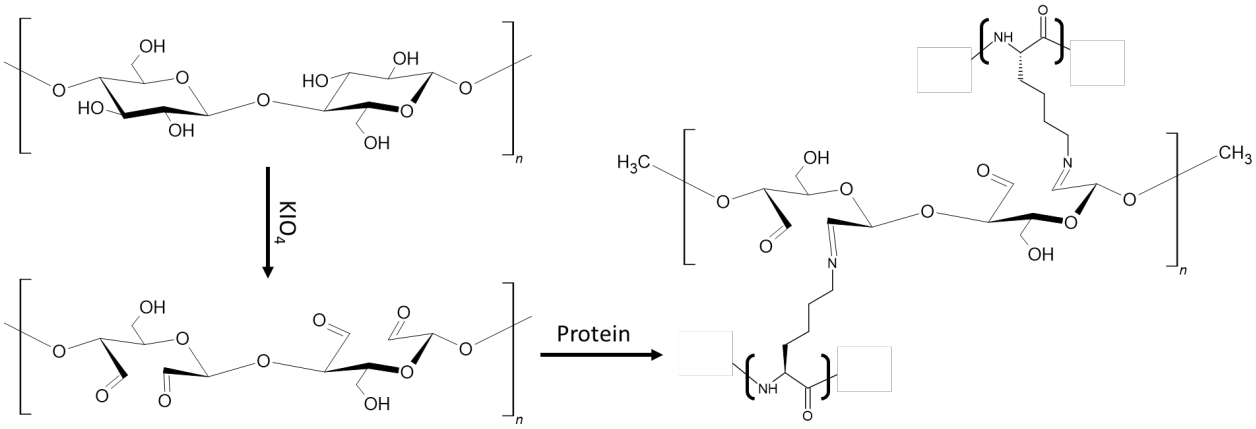

Figure 2: Reaction of Cellulose with Potassium Periodate. KIO_4 oxidizes carbons 2 and 3 of each glucose monomer, opening the ring and forming two aldehyde groups. Antibodies or other polypeptides can then react with those aldehydes (via n-termini or lysine groups) to form Schiff bases causing them to adhere firmly to the cellulose material.

to the oxidized cellulose, and the aldehydes will form Schiff bases with amines (from lysine's or N-termini) from the protein. These strong bonds make oxidized cellulose an excellent platform for protein immobilization in a host of potential applications.

Oxidized cellulose has been studied extensively for its physical, chemical, and biological properties. Oxidized cellulose can effectively bind and immobilize trypsin[12,13], catalase[14], hormones[15], and antibodies[16–18]. Because of its ability to immobilize antibodies, oxidized cellulose is a fantastic material to use in immuno-bio-diagnostics. Previous publications have used oxidized cellulose to immobilize antibodies for various bio-diagnostics, including ELISA's[18], colorimetric paper discs[19], and even electrochemical immunosensors[20]. Another study used an oxidized cellulose cotton swab to immobilize lactoferrin and then use those lactoferrin swabs to probe for bacteria on surfaces in a colorimetric assay.[21]

We decided to explore the oxidation of easily accessible cellulose materials made from cotton and other plant fibers and probe their ability to function in an immunological sandwich assay. By characterizing easy-to-find materials found in almost every country on Earth, we hope to provide more accessible methods and materials for anyone to develop their own POC assays. Due to the ease of manufacturing and flexibility of use, we chose to characterize cotton balls, printer paper, several different kinds of cotton fabrics, rayon fabric, and hemp string.

Experimental

Periodate Oxidation - General

1 liter of 0.03 M KIO4 was prepared on the day of use by adding 6.9 g KIO4 1 liter of distilled/deionized water. This solution was loosely capped and mixed with a magnetic stir bar on a hot plate at 90 °C until all KIO4 was utterly dissolved (about 45 minutes). Each cellulose material

was submerged in KIO4 solution and incubated for 2 hours at 65 °C. Excess KIO4 was removed, and the oxidized cellulose was washed three times with distilled water and left out to dry at room temperature.

FTIR

Fourier Transform Infra-Red (FTIR) spectroscopy was performed on a Nicolet 6700 FTIR spectrometer (Thermo Scientific) using a Small Orbit Diamond ATR apparatus (Thermo Fisher) with an absorbance range between 30,000-200 cm-1. 50 scans measuring absorbance at a resolution setting of 6 were performed for each cellulose material and its oxidized derivative. OMNIC™ (Thermo Fisher) IR analysis software was used to analyze and superimpose peaks. The appearance of a peak at 1740-1720 cm-1 indicated the presence of aldehyde carbonyls and suggested successful oxidation of cellulose to dialdehyde cellulose.

Immobilization of Antibodies

5 µL of goat anti-mouse antibodies (Invitrogen catalog#: 31160) were pipetted onto a small piece of each oxidized material and nitrocellulose. These materials were dried entirely and then the cotton substrate with any remaining activated aldehyde functional groups was inactivated by blocking for 1 hour by shaking the cotton substrate in 5% powdered milk in distilled deionized water. At the end of 1 hour, the milk was removed and the materials were rinsed three times in distilled water. The cellulose material conjugated to antibodies was stored at 4 °C.

Dot Blot Sandwich Assay

To test for binding, anti-mouse immobilized materials were soaked in 5 mL of 10% v/v of a gold nanoparticle solution conjugated to mouse anti-HCG antibodies (Fitzgerald catalog#: 62-H25C) in TBS-T (Tris Buffered Saline-Tween-20) for 1 hour shaking. Gold-solution was removed,

and materials were rinsed three times with distilled water. Materials were dried overnight at room temperature. Gold staining was imaged on Canon CanoScan 8800F scanner at 1200 DPI, and contrast was adjusted to give optimal intensity.

Cotton Swab Test

Cotton swabs were oxidized as described and treated with 3 µL of goat anti-mouse antibodies near the shank and 3 µL of mouse anti-HCG antibodies (MyBioSource catalog#: MBS832263) at the tip. Cotton swabs were blocked and dried as before. Cotton swabs were tested in 1 mL of 10% v/v gold-mouse-anti-HCG in TBS-T with a tenfold serial dilution of HCG: 10,000 ng/mL, 1,000 ng/mL, 100 ng/mL, 10 ng/mL, 1 ng/ml, and compared to a control of 0 ng/mL. These soaked for 3 hours and were then rinsed three times in distilled water. Pictures of cotton swabs were taken using a phone camera

Hemp String Test

Hemp string was oxidized as before, treated with 5 µL of anti-mouse antibody and 5 µL of anti-HCG antibody, and blocked as before. This exposed string was placed in 100 µL 10% v/v gold-mouse-anti-HCG TBS-T with 10,000 ng/mL, 1,000 ng/mL, 100 ng/mL, 10 ng/mL, 1 ng/ml, and a control of 0 ng/mL of HCG. These tests were allowed to sit for 10 minutes, wicking up the test fluid. At the end of ten minutes, the tests were rinsed with distilled water three times. Gold staining was imaged on the Canon CanoScan 8800F scanner at 1200 DPI, and contrast was adjusted to give optimal intensity.

Cotton Tube Test

Small pieces of cotton fabric were oxidized as described, treated with 5 µL of anti-mouse antibody or 5 µL of anti-HCG antibody, and blocked as before. When dry, these cotton pieces were bunched up and inserted into a clear plastic tube, and then held into place with smaller plastic tubes. Each plastic tube made contained one anti-mouse piece of cotton and one anti-HCG piece of cotton. These tests were run by pushing 1 mL of 10% v/v gold-mouse-anti-HCG in TBS-T through the tube with 10,000 ng/mL, 1,000 ng/mL, 100 ng/mL, 10 ng/mL, 1 ng/ml, or a control with 0 ng/mL HCG present. This 1 mL solution was pushed over the cotton 5 times with a syringe, and then the test was rinsed with 15 mL of distilled water. Gold staining was imaged on the Canon CanoScan 8800F scanner at 1200 DPI, and contrast was adjusted to give optimal intensity.

Results

Periodate Oxidation

Eleven different cellulose materials were oxidized using KIO_4, a potent oxidizing agent. These materials included cotton balls, printer paper, duck canvas, flannel, cheesecloth, sateen, bull denim, twill, hemp string, and lyocell/rayon. FTIR was used to confirm that these materials were successfully oxidized by monitoring for aldehyde groups' presence in the material (figure 3). The appearance of a peak at 1740-1720 cm-1 indicated the presence of aldehyde carbonyls and suggested successful oxidation of cellulose to dialdehyde cellulose. All materials showed the presence of aldehyde groups to varying degrees when oxidized.

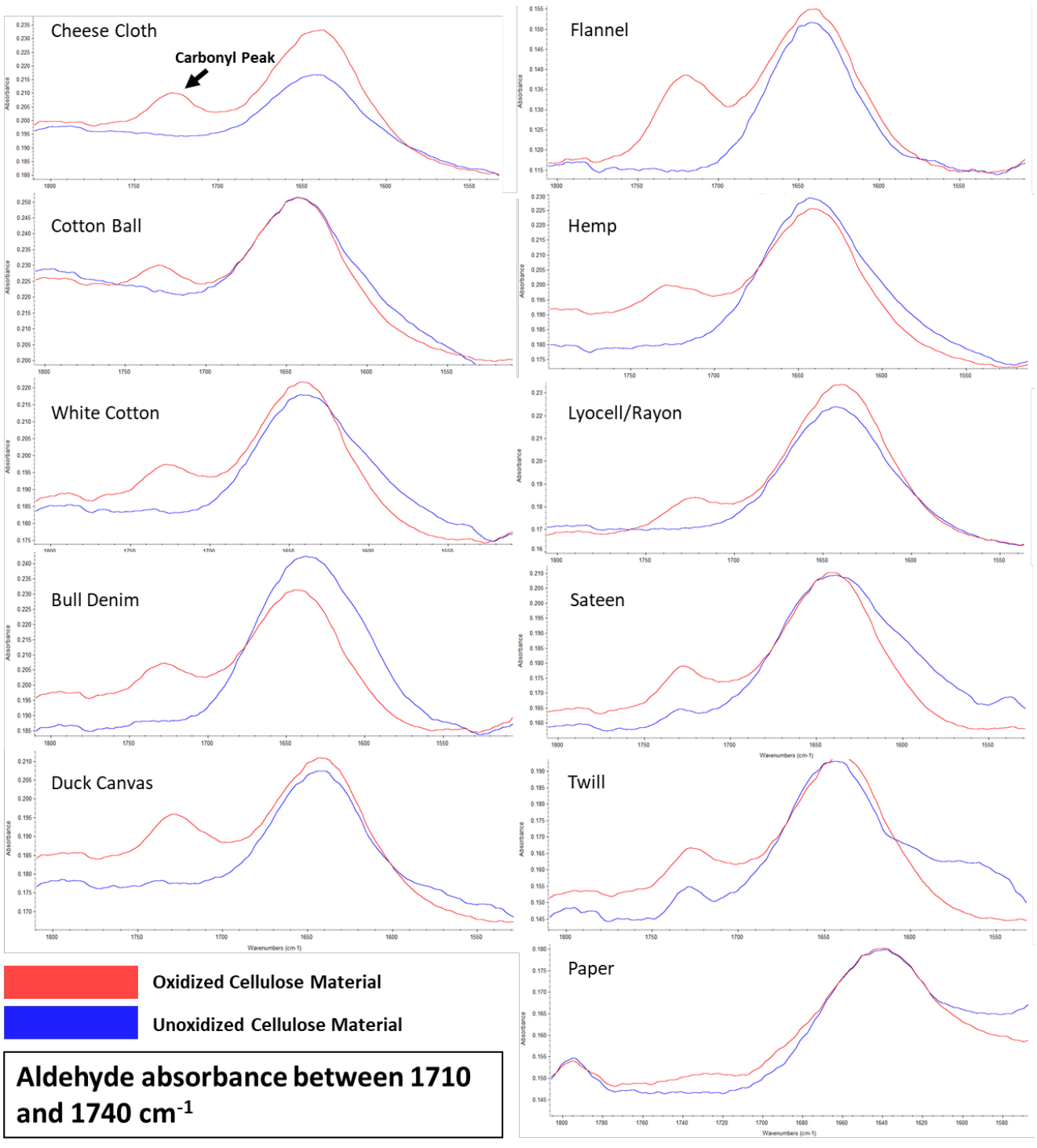

Figure 3: FTIR of Oxidized Cellulose Materials. Each of the listed cellulose-based materials were oxidized and compared to unoxidized material using FTIR. The appearance of aldehyde IR absorbance between 1710 and 1740 cm-1 indicated that the material had been successfully oxidized when compared to the spectra from unoxidized cellulose.

Sandwich Assay Characterization

We confirmed that each of the 11 oxidized materials can bind antibodies by immobilizing anti-mouse antibodies to each material and incubating them with gold nanoparticles conjugated to antibodies from mice (figure 4). We also included a nitrocellulose membrane in our trials as a comparison. Every material stained pink where the antibodies had been added, indicating that the antibodies had been successfully immobilized. The staining pattern for each had a different shape and spread depending on the density of the material and the tightness of the weave.

We then chose a subset of these materials to create new tests in a sandwich assay format, probing for HCG, the pregnancy hormone. We decided to probe for HCG because it is the focus of pregnancy tests which makes it an extremely well-developed area of bio-diagnostics with

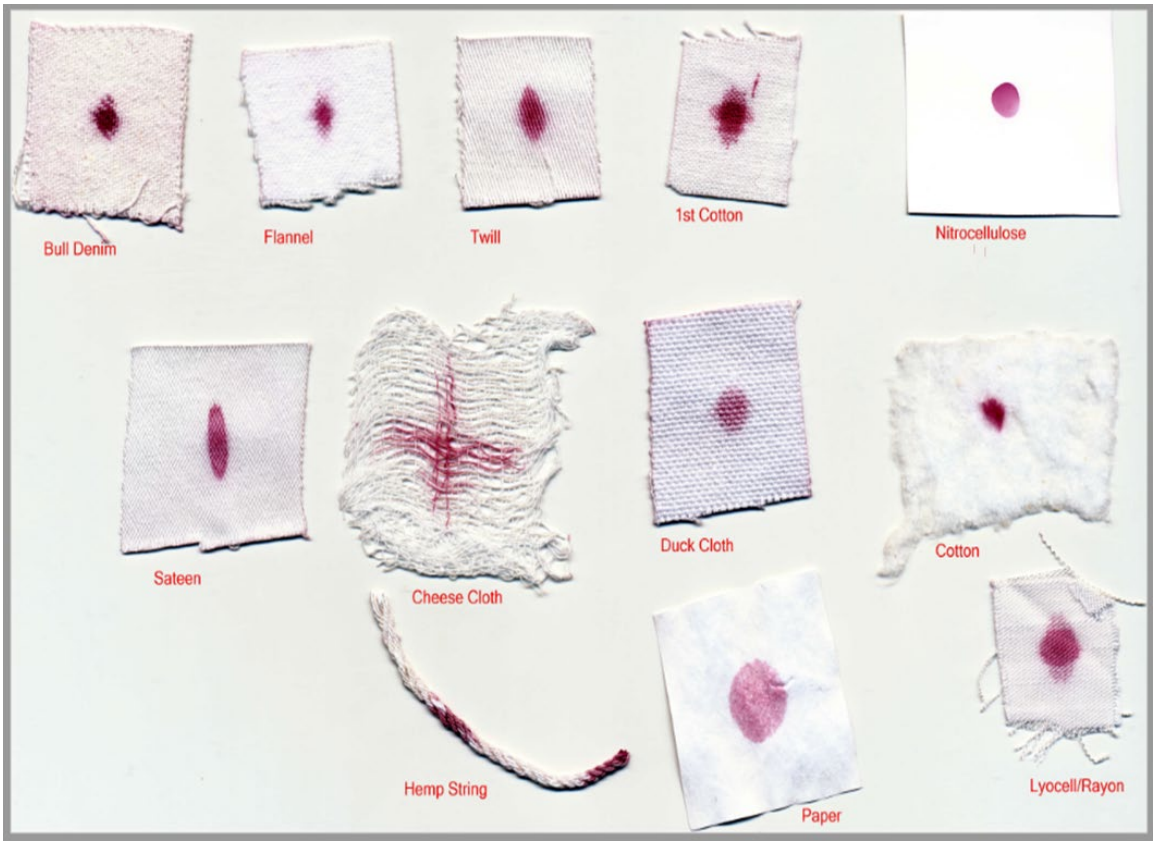

Figure 4: Test of Oxidized Cellulose Materials. The above oxidized cellulose materials dotted with anti-mouse antibodies were treated with gold nanoparticles conjugated to mouse antibodies for one hour. This resulted in the colorimetric readout seen above.

readily available supplies. This allowed us to easily compare the efficiency and efficacy of these materials we tested to market available LFI's. These tests are described in the following three sections.

Cotton Swab Test

Using the materials we characterized above, we set out to make and characterize new POC platforms utilizing immunological sandwich assays focusing on HCG as a model, but with the hope that they could be applied to any analyte in the future. The first assay we created was the cotton swab immunoassay (figure 5). Here we oxidized a cotton swab on a wooden shaft and immobilized anti-mouse antibodies close to the shaft (as a positive control) and anti-HCG antibodies at the tip. This assay was performed by placing the cotton swab in a solution containing

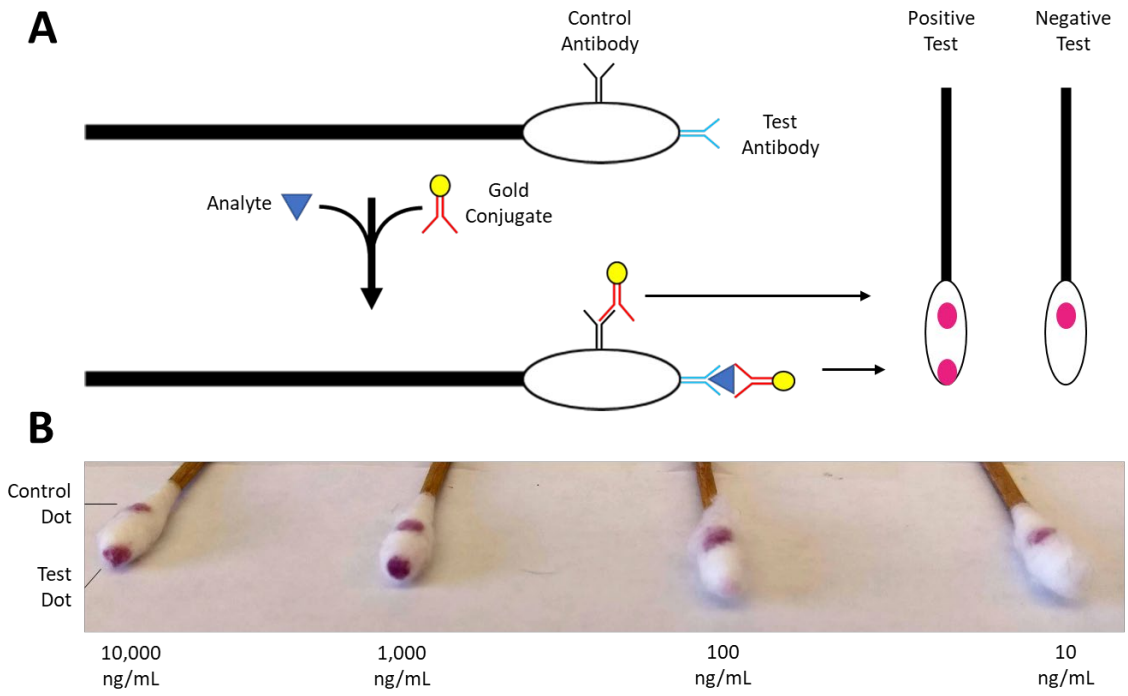

*Figure 5: Cotton Swab Test. **A**: Schematic showing oxidized cotton swab immobilized with test antibodies against the analyte of choice and control antibodies against the conjugate antibodies. When analyte and gold-nanoparticles conjugated to an antibody against that analyte are incubated with the cotton swab test, two pink dots appear indicating a positive test. If no analyte is present, only the control dot will appear indicating a negative test. **B**: Limit of Detection of Cotton Swab Test For HCG. Oxidized cotton swabs dotted with anti-HCG antibodies and anti-mouse control antibodies were placed in solutions containing varying amounts of HCG mixed with mouse-anti-HCG antibodies conjugated to gold nanoparticles. The lowest signal obtained in these tests came from a 100 ng/mL HCG in solution.*

HCG and gold nanoparticles for 2 hours. When removed and washed, the presence of two dots meant the test was positive. The appearance of one dot meant the test was negative. We performed a limit of detection assay on the cotton swab test and found that the cotton swabs could faintly detect as low as 100 ng/mL of HCG (figure 5B).

String Test

The second assay we created was based on hemp string. We immobilized anti-mouse and anti-HCG antibodies on an oxidized hemp string (figure 6). This test was placed with the end of

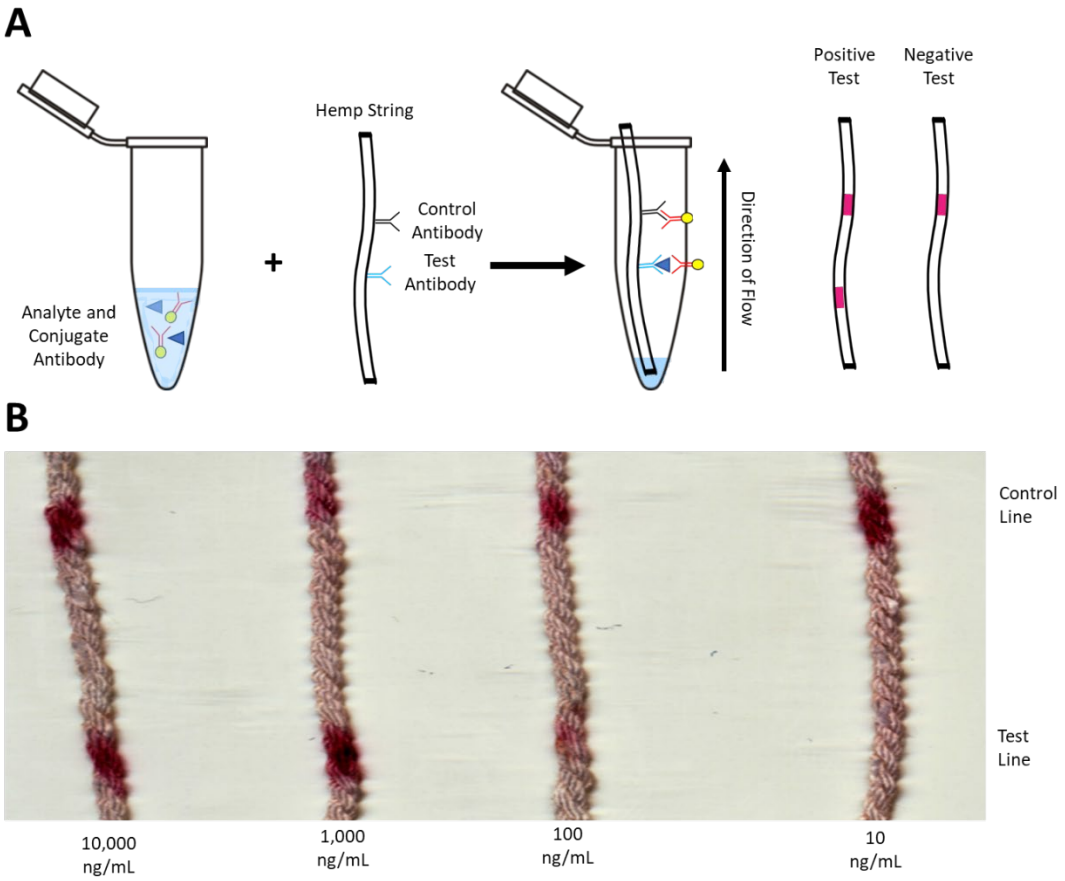

Figure 6: Hemp String Test. ***A:*** *Schematic showing oxidized hemp string immobilized with test antibodies against the analyte of choice and control antibodies against the conjugate antibodies. When analyte and gold-nanoparticles conjugated to an antibody against that analyte are incubated with the hemp string, two pink lines appear indicating a positive test. If no analyte is present, only the control dot will appear indicating a negative test.* ***B:*** *String Test Limit of Detection with HCG. Oxidized hemp string tests dotted with anti-HCG antibodies and anti-mouse control antibodies were placed in solutions containing varying amounts of HCG mixed with mouse-anti-HCG antibodies conjugated to gold nanoparticles. The lowest signal obtained in these tests came from a 100 ng/mL HCG in solution.*

the string hanging in 100 µL solution of HCG and gold nanoparticles. The solution was then allowed to wick up the hemp string for 10 minutes until all liquid was gone. The string was then rinsed with water to reveal the gold stains. Two stains indicated a positive test, while one stain indicated a negative test. We also performed a limit of detection assay on the hemp string test and found that it could detect as low as 100 ng/mL of HCG (figure 6B).

Cotton Tube Test

The third assay we created used small pieces of cotton fabric immobilized with either anti-mouse or anti-HCG antibodies. For each test, one anti-mouse, one anti-HCG, and one blank piece of cotton were bunched up and inserted into a clear plastic tube and held into place with clear plastic inserts (figure 7). This test was run by pushing 1 mL of a solution of HCG and gold nanoparticles conjugated to anti-HCG antibodies through the tube five times with a syringe and

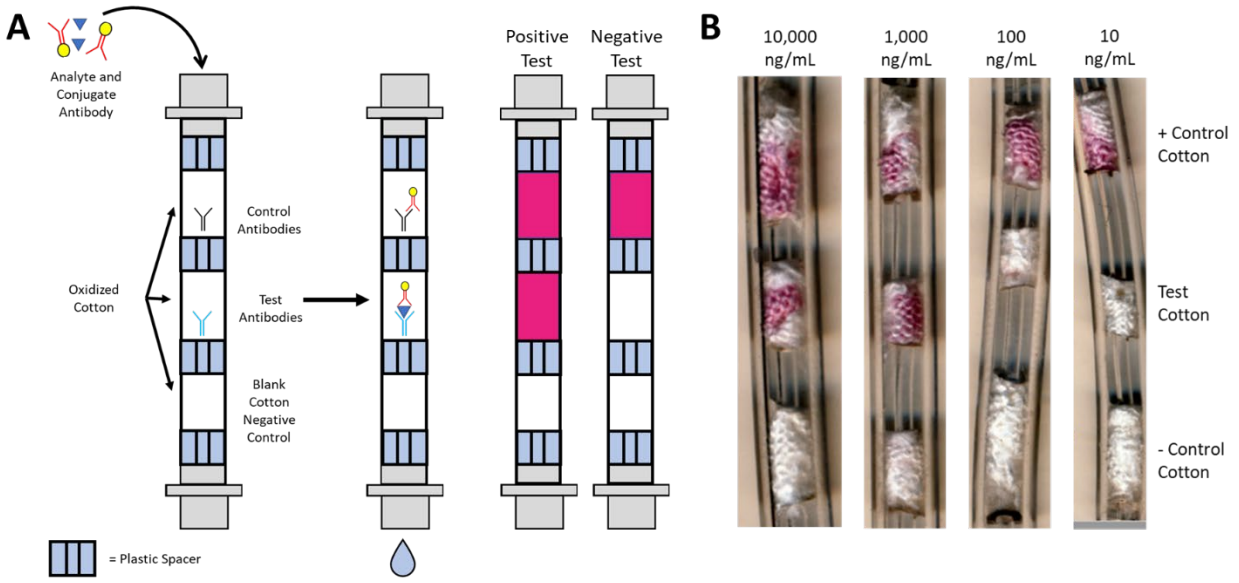

Figure 7: Cotton Tube Test. ***A:*** *Schematic of showing oxidized pieces of cotton immobilized with test antibodies against the analyte of choice and control antibodies against the conjugate antibodies and control antibodies packed into a clear plastic tube and held in place by plastic spacers. When analyte and gold-nanoparticles conjugated to an antibody against that analyte are pushed through the test with a syringe, two pieces of cotton will turn pink indicating a positive test. If no analyte is present, only the control piece of cotton will turn pink indicating a negative test.* ***B:*** *Limit of Detection of Cotton Tube Test for HCG. Cotton tube tests containing cotton dotted with anti-HCG antibodies and anti-mouse control antibodies were run through solutions containing varying amounts of HCG mixed with mouse-anti-HCG antibodies conjugated to gold nanoparticles. The lowest signal obtained in these tests came from a 1,000 ng/mL HCG in solution.*

then rinsing it with water until the blank negative control was white again. The test was positive if the top two cotton pieces remained stained and negative if only one piece of cotton remained stained. We also performed a limit of detection assay on this cotton-in-a-tube test and found that it could detect as low as 1000 ng/mL of HCG (figure 7B).

Discussion

In this chapter, we established that many different kinds of cellulose-based materials could easily be oxidized and used as a platform for antibody immobilization in immunological sandwich assays. We also provided three examples of possible POC assays that can be made with these materials and demonstrated their potential effectiveness by providing their limit of detections for HCG. The threshold of HCG present in a sample for a woman to be considered pregnant is 24 mIU or approximately 2,400 ng/mL. All of our oxidized cellulose assays detected well below this mark, showing that these tests could be viable in a real-world setting. We only tried one antibody pair that was known to work well for HCG in these experiments. The detection limits for disease-relevant biomarkers with different antibody pairs could obtain an even lower limit of detection.

We developed these three tests in the course of 6 months with only the cellulose materials, potassium periodate, antibodies, and gold nanoparticles. I believe that these and other tests could easily be developed by low-income laboratories because no specialized equipment was required for the development. The main hurdle in resource-poor areas would be obtaining antibodies for the antigen of choice. Still, with ever-expanding antibody industries, I hope that antibodies will continue to lower in cost and become more available to low-income areas. It is also possible that the World Health Organization or humanitarian agencies could aid these countries to purchase antibodies to make POC tests.

The cost of materials for the cotton swab test, hemp string test, and cotton tube test were all very low, with most of the cost coming from the antibodies and pre-conjugated gold nanoparticles in each case. Admittedly, antibodies make up the bulk cost of most immune-diagnostics. Mass production of these tests could help bring down these antibody costs.

Further exciting possibilities exist for the POC assays we have presented here. The cotton swab test could potentially be used as both a means to collect a sample from a surface (a tabletop, toilet seat, oral cheek swab, or nasopharyngeal swab) and to act as the actual test itself. This would decrease complexity and increase user ease-of-use. With its increased absorbency, the hemp string test could be used in situations where LFI's cannot wick analyte quickly, such as saliva or other complex vectors. Additionally, one could imagine an LFI made of one of these oxidized cellulose materials, eliminating the need for sample or absorbance pads due to these cellulosic materials' natural absorbency. Of course, further testing will need to be done to ensure that each of these possibilities would work in user-friendly ways.

CHAPTER 2: Fast Flow Immunoassays (FFI's)

Introduction

One of the significant limitations that frequently comes up during LFI development is that of sensitivity. The most significant factor determining how sensitive an LFI or other sandwich assay will be is how sensitive the antibodies are. The process of choosing suitable antibodies needs to be well thought out and carefully tested. There are, however, other ways to increase sensitivity if the sensitivity of a given pair of antibodies is lacking. One issue that LFI's have is that there is only one relatively short chance for the analyte to bind to the test strip. Analyte gets one chance, and if the flow is too fast or the binding too weak, the signal will also be weak. One way to increase signal would be to allow the analyte multiple opportunities to bind to the immobilized antibodies on the test strip. This chapter describes our attempts to create a more sensitive test that bypasses the need for a one-pass capture by capillary action. This was done by passing the sample over the capture antibodies multiple times.

We designed a test platform that would be able to meet the needs described above. It consists of a syringe filter adaptor encasing a nitrocellulose filter immobilized with antibodies. In this test, a sample is forced through the disk using a syringe, making the test rely on hand power rather than capillary action. After being pushed through once, a sample can be run through the test additional times with minimal effort to increase the opportunities that the analyte has to bind with the capture antibodies. We named this POC assay that we created the Fast Flow Immunoassay (FFI) (figure 8).

The FFI syringe filter head consists of two adaptors that can be threaded together. The top piece has a Luer-lock adaptor for attachment to a plastic syringe. The bottom piece has a skinny dispenser from which sample is expelled. A sieve supports a nitrocellulose filter containing immobilized antibodies in the middle where the two pieces thread together. The metal sieve and the nitrocellulose filter are locked in place with O-rings when the two parts are threaded together. This test is run by taking up the analyte mixed with gold nanoparticles conjugated to antibodies specific to that analyte in a syringe. This mixture is then pushed through the metal syringe filter. The eluted liquid is collected in a tube on the other end and can be passed through the filter multiple times to increase the signal. This test's signal will appear as a pink dot on the nitrocellulose due to the aggregation of gold nanoparticles forming an immunological sandwich between the nitrocellulose, capture antibody, analyte, conjugate antibody, and gold nanoparticle.

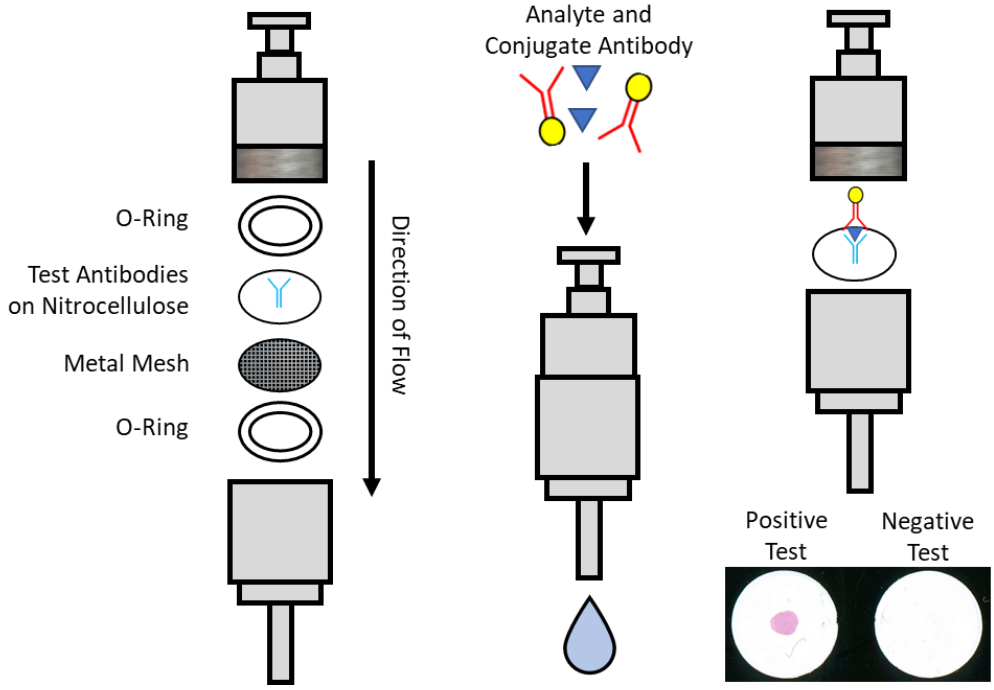

Figure 8: Fast Flow Immunoassay Schematic. The FFI filter head from top to bottom consists of a metal casing with a luer lock adaptor, an O-ring, a nitrocellulose filter dotted with antibodies against an analyte, a metal filter, another O-ring, and the rest of the metal casing with a dispensing end. These are assembled by threading the two ends together. The test is run by pushing analyte and gold nanoparticles conjugated to antibodies against that analyte through the filter head with a syringe. This can be repeated multiple times to increase signal. When complete the nitrocellulose filter is removed, if a pink dot has formed, it is a positive test; if not it is a negative test.

We tested the FFI in its ability to increase signal and sensitivity in a given test. We also compared the sensitivity of FFI's to a dot blot sandwich assay on nitrocellulose using the same antibodies and gold nanoparticles in both tests. Finally, we found the limit of detection of our FFI when using antibodies to detect HCG, the pregnancy hormone.

Experimental

Immobilization of Antibodies on Nitrocellulose Discs

5 µL of goat anti-mouse (Invitrogen catalog#: 31160) or mouse anti-HCG (MyBioSource catalog#: MBS832263) antibodies were added to a small circular disc of nitrocellulose 11 mm in diameter. These discs were dried entirely and then blocked for 1 hour, shaking in 5% Milk. At the end of 1 hour, the milk was removed and the discs were rinsed three times in distilled water. These were then placed at 4 °C overnight to dry.

FFI Multipass Test

A nitrocellulose disc was placed in the syringe adaptor on top of the metal sieve and locked into place on either end with O-rings as the adaptor is threaded together. 1 mL of 10% v/v gold-nanoparticle-mouse-anti-HCG (Fitzgerald catalog#: 62-H25C) in TBS-T was taken up in a 15 mL plastic syringe. This solution was pushed through a syringe filter at a slow constant rate and collected in a tube. These steps were repeated with the original solution multiple times to determine if multiple passes of a sample over the filter increased the intensity. When complete, 10 mL of distilled water was run through the syringe filter to remove excess gold, and the nitrocellulose filter was removed.

Dot Blots

Dot blots for comparison were completed by incubating nitrocellulose discs immobilized with anti-mouse antibodies with 10% v/v gold-nanoparticle-mouse-anti-HCG in TBS-T. These were incubated for 1, 3, 10, 20, 30, or 60 minutes. Each disc was washed three times in distilled water and dried completely.

Limit of Detection

The limit of detection of anti-HCG FFI's was tested by running those FFI's as described above with three passes each. These tests were run on serial dilutions of HCG: 10,000 ng/mL, 1,000 ng/mL, 100 ng/mL, 10 ng/mL, 1 ng/ml, and a control of 0 ng/mL. These tests were washed three times in distilled water and dried completely. A pink dot indicated a positive test.

Scanning Tests

Gold staining was imaged on the Canon CanoScan 8800F scanner at 1200 DPI, and contrast was adjusted to give optimal intensity. Scans were quantified using ImageJ software, measuring each dot's average intensity, and normalizing that intensity to the average intensity of a blank nitrocellulose filter. The resulting graphs show how many times more intense each test is than a blank white nitrocellulose disc.

Results

Multipass Test vs Dot Blot

We tested how FFI's could increase a test's signal by passing a sample through the filter multiple times. We used nitrocellulose immobilized with anti-mouse antibodies and ran a solution of gold nanoparticles conjugated to mouse-antibodies through it 1-10 times (figure 9). It took about

one minute to pass the sample through the FFI filter one time. We observed a linear increase in signal intensity for each additional pass, showing the ability FFI systems have to easily increase signal intensity. We compared these samples to the sample nitrocellulose filters run on a dot blot time course for up to an hour and found that the signal from the FFI system with only one pass

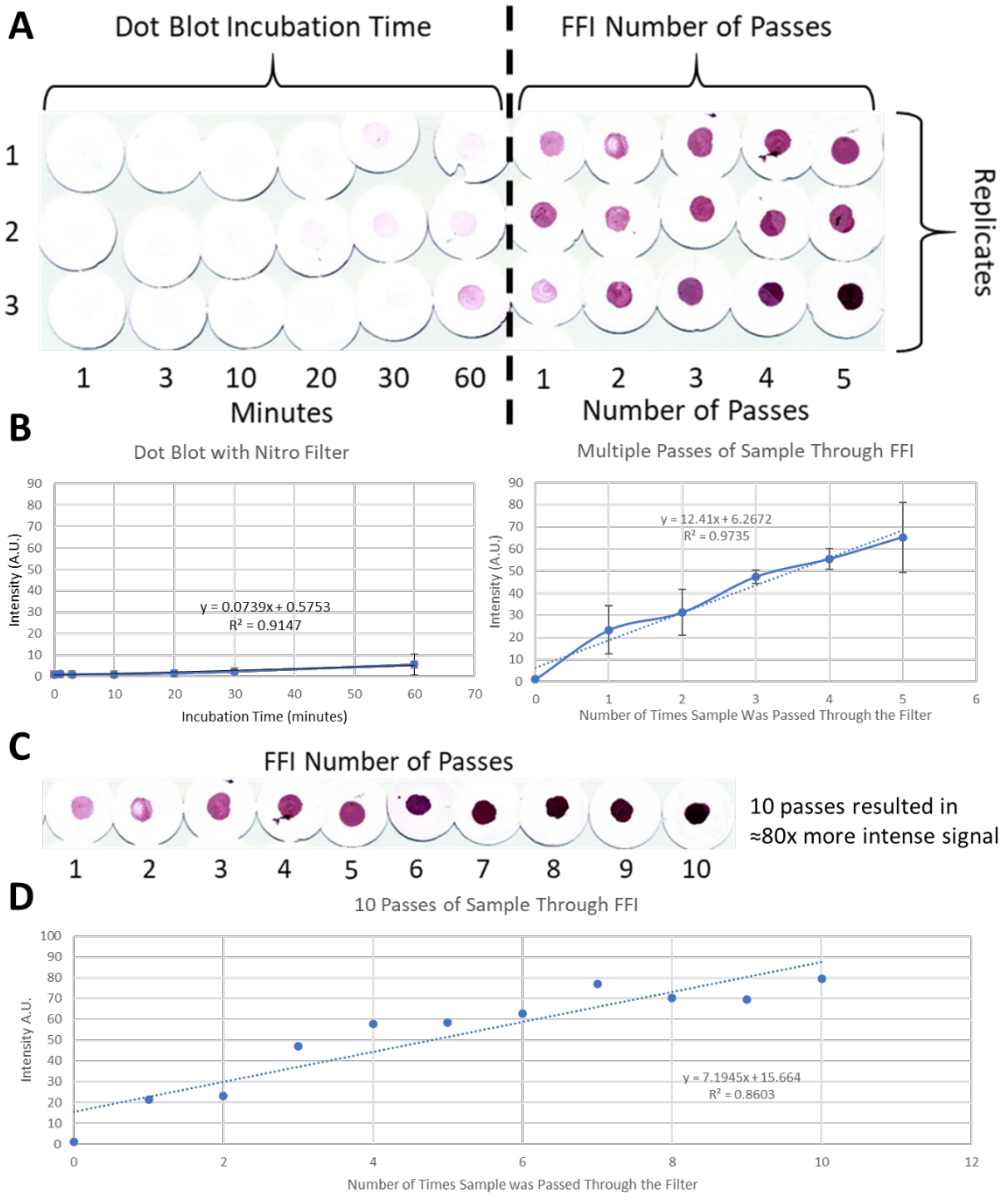

Figure 9: Increasing FFI Signal with Multiple Passes. ***A:*** *The ability of the FFI system to increase signal by passing sample over a nitrocellulose filter fixed with antibodies was tested with anti-mouse antibodies, and gold nanoparticles conjugated to mouse antibodies. All filters shown are separate filters with the indicated number of passes. A dot blot with the same filters and antibodies was done for 1 hour for comparison.* ***B:*** *The quantification of the dot blots and multi-pass test.* ***C:*** *Multi-pass test up to 10 passes of the sample through the filter. 10 passes resulted in ≈80x greater signal than a blank filter.* ***D:*** *Quantification of those 10 passes.*

was more than four times greater than the dot blot signal at 1 hour and that an FFI with five passes had almost 12 times greater intensity, all while taking five minutes or less. These experiments show that our fast flow system is both rapid and sensitive.

Limit of Detection of HCG FFI

We tested the limit of detection of the FFI system using a set of antibodies known to work well to detect HCG in a sandwich assay. We found that the FFI with three passes could detect as little as 100 ng/mL of HCG (figure 10). It took on average 3 minutes to obtain results for these tests. As a comparison, we tested a commercially available LFI for HCG produced by Clinical Guard in the same conditions. These HCG LFI's and our FFI's are not directly comparable because they use different antibodies and gold nanoparticles. Even so, it was still usefully to compare the FFI test against a market-ready test for HCG. The HCG LFI test took about the same amount of

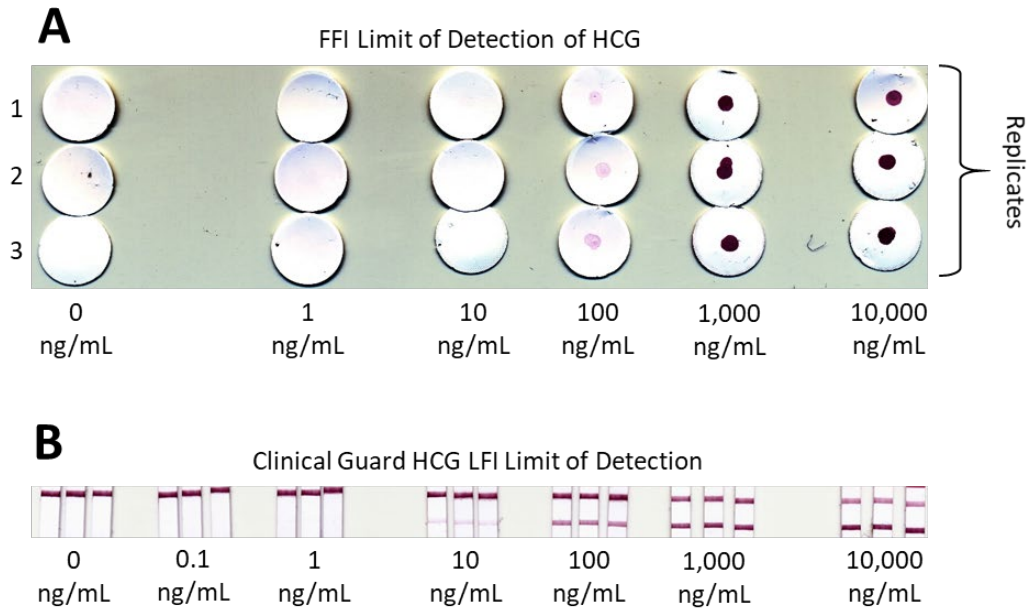

Figure 10: FFI Limit of Detection for HCG. Nitrocellulose filters immobilized with anti-HCG antibodies were tested against various concentrations of HCG mixed with gold nanoparticles conjugated to additional anti-HCG antibodies. This solution was passed through the filter 3 times. These tests were run in triplicate The lowest signal obtained in these FFI's was 100 ng/mL HCG. Clinical Guard HCG LFI tests available on the market were run under the same conditions for comparison. These were able to detect as low as 10 ng/mL but did not use the same antibodies as the FFI.

time to run as the FFI and had a lower limit of detection at 10 ng/mL. We suspect that these differences are mainly due to differing antibody affinity, but this fact will need to be tested.

Discussion

We found the fast flow immunoassay system described here to be a rapid and sensitive assay. The FFI was more sensitive to HCG than the dot-blot sandwich assay because it forced the analyte through a small area, making it come in close contact with the capture antibodies (similar to how LFI's focus analyte through a small area via capillary action). The FFI also proved to be more sensitive because the analyte could be passed through the filter multiple times, increasing the signal with each pass.

In the experiments detailed above, we modeled the FFI in an ideal buffer situation. It would be interesting to compare the functionality of an LFI and an FFI with the same antibody pairs in different biological buffers (i.e. saliva, urine, serum). Testing other buffers would allow us to see if the FFI would outperform the LFI in buffers that have traditionally been difficult to use in capillary flow-based tests. Similarly, testing actual biological samples using the same two tests will allow us to determine if there is a limit of detection benefit for patients. Even if the limit of detection is identical, the faster results will allow the FFI to become an important method to use.

Combining ideas from chapter one and this chapter, it would be possible to make an FFI system that utilizes an oxidized cellulose filter instead of nitrocellulose. We briefly tested this possibility (data not shown) and found that oxidized cotton works just as quickly in an FFI system as nitrocellulose. The use of oxidized cellulose in FFI's is another avenue that can be explored in the future to reduce the cost of this test and perhaps increase the ease-of-use by using materials that samples can flow through easily.

One great benefit that FFI systems could have is facilitating quicker development of POC bio-diagnostics in times of need. When a new biomarker for a disease is discovered (like the spike protein of SARS-CoV-2), antibodies must first be raised against that bio-marker before immunological-based assays can be developed. These antibodies are made by injecting the new bio-marker into animals and waiting for the animal to develop them. The first antibodies produced from this process are usually weak with low binding affinities. Over time antibodies with higher binding affinities can be produced, but this takes time, and making more robust antibodies is not always possible. The FFI could help these weaker antibodies function in POC assays because of its ability to improve a test's sensitivity by running the sample multiple times. Helping weaker antibodies perform in POC assays would facilitate quicker development of important tests by assisting early iterations of ineffective antibodies to be sensitive enough.

SECTION 2: GOLD NANOPARTICLES AS A MEDICINE

BACKGROUND

The concept of gold as a medicine is not a new one. Though traditionally valued for its inert and non-reactive character, gold can be a very effective catalyst at the nano and molecular level, as in the case of nanoporous gold.[22] Early unsuccessful applications of gold in medicine attempted to treat tuberculosis with gold.[23] Later on, it was found that gold as a part of an organic molecular platform could successfully treat autoimmune and inflammatory diseases such as rheumatoid arthritis.[24]

In the last decade, gold nanoparticles have been used as a platform to carry treatments to treat a variety of diseases. Gold nanoparticles have been used as non-toxic carriers of drugs and nucleic acids to tumor sites for various kinds of cancer.[25–28] They have also been used in photothermal therapy, in which a tumor treated with gold nanoparticles is irradiated with laser light exciting the gold nanoparticles, causing an increase in temperature and killing the cancer cells as a result.[28] It has also been hypothesized that gold nanoparticles themselves could inhibit angiogenesis, staving off tumors' growth.[28]

Gold nanocrystals are a special category of gold nanoparticles in which particles are formed by the nanocrystalline assembly of gold. Gold nanocrystals appear to have more catalytic abilities than normal spherical nanoparticles due to their edges and corners.[29,30] Recently a uncapped catalytic gold nanocrystal was reported by Robinson et al. to be able to treat Multiple Sclerosis, a neurodegenerative disease caused by the demyelination of neuronal axons .[31] This gold nanocrystal was shown to catalyze the oxidation of NADH to NAD^+. Its ability to catalyze this reaction was implicated in its ability to facilitate remyelination in models of multiple sclerosis.[31] Because of those encouraging results, gold nanocrystals are currently undergoing phase II clinical trials other

neurodegenerative diseases including multiple sclerosis[32], Parkinson's disease[33], and Amyotrophic Lateral Sclerosis (ALS).[34]

While the above results are encouraging, they were pursued only in oligodendrocytes and in no other cell type. Additionally, little is known about molecular pathways that gold nanocrystals could be affecting directly or indirectly. We decided to investigate potential molecular pathways that gold nanocrystals could be affecting in liver tissue-cell culture to find new potential therapeutic effects or possible off-target effects. We chose to explore these interactions in liver cell culture because the liver is the center of metabolic activity in the body and essential in understanding drug-body interactions. The two molecular pathways we chose to explore based off of the literature were the IL-6/Jak/STAT3 inflammatory pathway, and the Nrf2 antioxidant defense pathway.

In addition to investigating molecular pathways that gold nanocrystals could be affecting, I decided to explore their direct protein interactors, the protein corona, in a proteomic style experiment. By ascertaining the composition of gold nanocrystals protein corona, I hoped to better understand their interactors and disposition. I decided to characterize this protein corona in fetal bovine serum (FBS) because FBS is an easily attainable model of human serum, and serum interaction can greatly determine the disposition and activity of a nanoparticle.[35]

CHAPTER 3: Effects of Gold Nanocrystals on pSTAT3 Inhibition

Introduction

Auranofin is a gold drug used to treat rheumatoid arthritis, a debilitating autoimmune disease in which the immune system attacks tissue surrounding the joints causing chronic inflammations and pain in individuals affected with the disease.[36] Auranofin is an S-glycosyl compound consisting of 2,3,4,6-tetra-O-acetyl-1-thio-β-D-glucopyranose with the sulfur atom coordinated to triethyl-phosphine gold (figure 11B). Studies have also shown that Auranofin may have some ability to treat HIV[37], Tuberculosis[38], Amebiasis[39], Ovarian cancer[40], and possibly COVID-19.[41]

In a 2007 paper, Kim et al. were able to show that Auranofin effectively inhibits the phosphorylation of STAT3 by JAK1 in liver tissue culture.[42] The Jak/Stat pathway is activated by Interleukin-6 (IL-6) which regulates inflammation, proliferation, and differentiation of many different types of cells.[43] This pathway plays a key role in causing chronic inflammatory pain in rheumatoid arthritis and other chronic inflammatory diseases.[44] The pathway is triggered when IL-6 cytokine binds to the membrane receptor GP-130 causing dimerization and autophosphorylation of the associated JAK kinase. The JAK kinase then phosphorylates STAT3 at Tyr705 and Ser727, causing dimerization and translocation to the nucleus. In the nucleus, the STAT3 dimer acts as a transcription factor upregulating genes involved in inflammatory and other pathways. This pathway scheme is shown here in figure 11a. Kim et al. were able to show that Auranofin inhibited the phosphorylation of STAT3 by JAK1 in a dose-dependent manner in cell culture that was treated with IL-6 (figure 11b). They found that these effects were negated when cells were co-incubated with thiolated small molecules, which would bind to the gold in theory. These results suggest that

Auranofin inhibits STAT3 phosphorylation by binding to some thiolated intermediate in that pathway.[42]

We hypothesized that other gold compounds could have a similar effect on liver tissue culture cells. Specifically, we thought that gold nanocrystals (with a diameter of 15 nm) might also be able to inhibit the phosphorylation of STAT3, especially because it would have a larger gold surface area with which thiolated intermediates could interact.

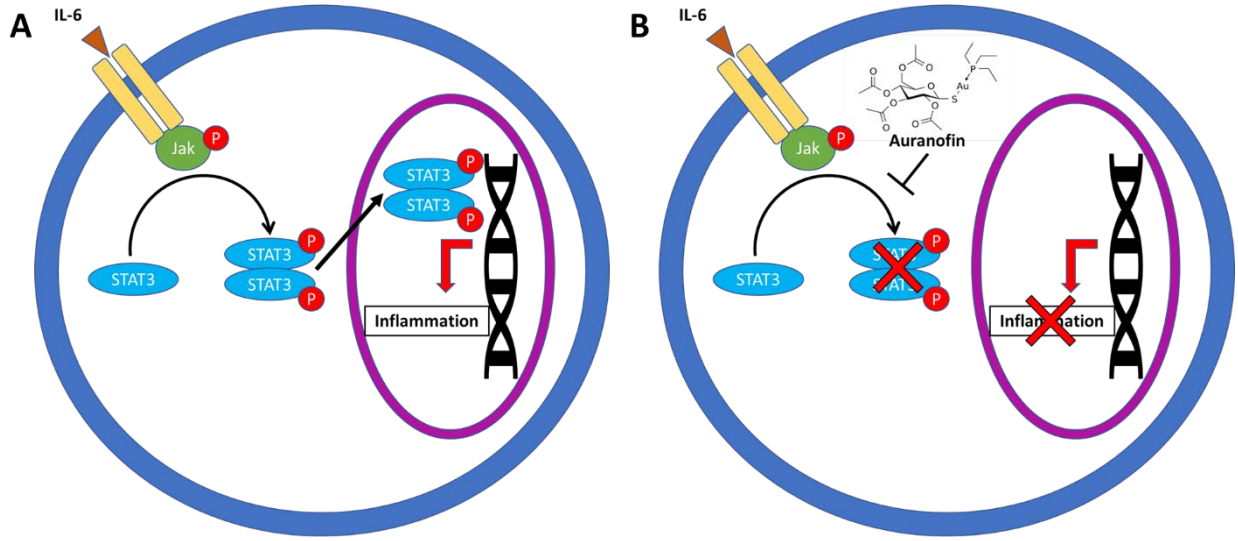

Figure 11: IL-6/Jak/STAT3 Inflammation Pathway. ***A:*** *IL-6 binds to cellular GP-130 transmembrane receptor inducing conformational changing activating and phosphorylating Jak Kinase. Jak kinase phosphorylates STAT3 causing it to dimerize and translocate to the nucleus. Once in the nucleus, the pSTAT3 dimer acts as a transcription factor activating genes that related to the inflammatory response.* ***B:*** *Auranofin, a gold-based drug is known to inhibit this pathway by preventing the phosphorylation of STAT3 to pSTAT3.*

Experimental

HepG2 Cell Culture and Treatment

HepG2 liver epithelial cells were cultured at 37 °C with Eagles Minimum Essential Medium (EMEM) supplemented with 10% FBS and 100 units/mL penicillin. Cells were maintained between 50% - 80% confluent and split at a 1:5 ratio when 80% - 90% confluent at low passage number (<20 passages). Cells were treated with 0.05% trypsin until adherence was

lost. The cellular solution was centrifugated at 1000 RPM for 4 minutes. The supernatant was discarded, and cells were resuspended in supplemented EMEM media. Resuspended cells were plated at 1/5 of their original concentration.

For treatment, cells were split and plated at a density of $5x10^6$ cells/mL and grown overnight. The following day cells were induced with 20 ng/mL IL-6 to induce the IL-6/Jak/STAT pathway and then treated with different concentrations of gold nanocrystals either concurrently or preemptively. Induced and treated cells were incubated at 37 °C for 24 hours unless otherwise noted.

Lysis

After treatment, media was removed, and cells were washed three times in sterile PBS buffer while on ice. Cells were isolated by centrifugation at 1000 rpm at 4 °C for 4 minutes, followed by removing the PBS supernatant. Cells were lysed by adding 200 µL RIPA buffer (150 mM NaCl, 50 mM Tris-Base, 0.5% Sodium Deoxycholate, 0.1% SDS, 1% Triton-X, one aliquot of HALT (Thermo Fisher catalog#78430) protease inhibitor cocktail/10 mL RIPA) and then flash-frozen in liquid nitrogen followed by immediate thawing in a 37 °C water bath. After thawing, the lysate was pipetted up and down 10x in a 22-gauge needle to shear the DNA. Samples were then centrifugated at 14,000 RCF for 30 minutes at 4 °C to pellet out the DNA.

Western Blotting

The amount of protein in each cell lysate was quantified using the protocol developed by Lowry et al.[45] Twelve bovine serum albumin (BSA) standards between 0 and 55 µg/mL were run in duplicate and used to quantify each sample that was run in triplicate. 25 µg of each sample was

combined with 5 µL of 5X loading dye (250 mM Tris-HCl pH 6.8, 10% SDS, 30% glycerol, 5% β-Mercaptoethanol, 0.02% Bromophenol Blue) and heated at 95 °C for 5 minutes. Samples were then centrifugated briefly and then added with a protein MW standard ladder (GoldBio #P007-500) to separate lanes in a 1.5 cm 5% acrylamide stacking gel on top of a 12% acrylamide Tris-SDS separating gel submerged in SDS-PAGE running buffer (25 mM Tris-Base pH 7.6, 200 mM Glycine, 1% SDS). Loaded gels were run at 150 V for 60 minutes or until dye had reached the end of the gel.

When SDS-PAGE gels had finished running, the gel was removed, rinsed with distilled water, and placed on a nitrocellulose membrane, and sandwiched between two pieces of filter paper and two sponges in a western blot cassette submerged in chilled transfer buffer (25 mM Tris-Base pH 7.6, 200 mM Glycine, 20% methanol). The western blot cassette was placed in a transfer tank filled with transfer buffer and chilled with ice. The protein was transferred from the gel to the nitrocellulose membrane at 0.25 Amps (constant current) for 90 minutes.

When the transfer was complete, membranes were removed, rinsed with TBS buffer (10 mM Tris-Base pH 7.6, 150 mM NaCl), and then dried for 15 minutes. Once dried, the membranes were rehydrated with distilled water and blocked in 5 mL of blocking buffer (10 mM Tris-Base pH 7.6, 150 mM NaCl, 5% powdered milk, 0.1% tween-20) shaking for 1 hour. At the end of 1 hour, 2.5 µL of anti-phospho-Stat3 (Cell Signaling Rabbit mAB #9145) and 5 µL of anti-β-actin (Cell Signaling Mouse mAB #3700) were added to the blocking solution and incubated at 4 °C shaking overnight. The next day the antibody solution was removed, and the blot was washed 3x for five minutes with TBS-T (10 mM Tris-Base pH 7.6, 150 mM NaCl, 0.1% tween-20). After washes, 5 mL of blocking buffer with 1 µL of anti-rabbit (Licor Donkey #926-32213 800 nm fluorescence) and 1 µL of anti-mouse (Licor Donkey #926-68072 680 nm fluorescence) secondary

antibodies conjugated to fluorescent probes was added to the blots to incubate for 1 hour. At the end of one hour, antibodies were removed, and the blots were rinsed three times with TBS buffer.

Western Blot Data Analysis

Blots were imaged on the LI-COR Odyssey® CLx scanner scanning for fluorescence at 680 nm and 800 nm. Images were processed and quantified using ImageStudio™ Lite software. Pixel intensity was calculated for bands of interest. Two pSTAT3 bands at 79 and 86 kDa were quantified in each lane on the 800 nm channel, and a single β-actin band at 42 kDa was quantified in each lane on the 680 nm channel. To normalize samples, the pSTAT3 intensity was divided by the β-actin intensity for every lane. For replicates across gels, each normalized intensity was divided by the normalized intensity of the IL-6 positive control. Averages and standard deviations were calculated for each sample across replicates. One-tailed heteroscedastic T-tests were calculated against the IL-6 positive control sample. P-values less than 0.05 were considered significant.

Results

Effect of Gold Nanocrystals on STAT3 Phosphorylation

To determine if gold nanocrystals can block the phosphorylation of STAT3 in a manner similar to Auranofin, we replicated the study by Kim et al. by inducing the HepG2 liver epithelial cells grown in tissue culture with IL-6 to turn on the JAK/STAT pathway. Cells were concurrently treated with varying concentrations of gold nanocrystals and then analyzed for pSTAT3 levels using western blotting. Figure 12A showed no reaction of pSTAT3 to the gold nanocrystals in the presence of IL-6 (250 ppm) when smaller doses of the nanocrystals ranging from 0.01 to 2 ppm

were used even as we confirmed that Auranofin effectively inhibits STAT3 phosphorylation. Figure 12B told a similar story with gold nanocrystal concentrations between 15 and 75 ppm. It wasn't until concentrations were increased to 250 ppm in figure 12C that a significant reduction in the levels of pSTAT3 was observed, suggesting that high concentrations of gold nanocrystals could inhibit the phosphorylation of STAT3. To confirm that lower concentrations did not affect pSTAT3, we performed a time course pre-incubating 1 ppm of the gold nanocrystals with HepG2 cells before the addition of IL-6. These results are shown in figure 12D and yielded no significant reduction in pSTAT3 levels.

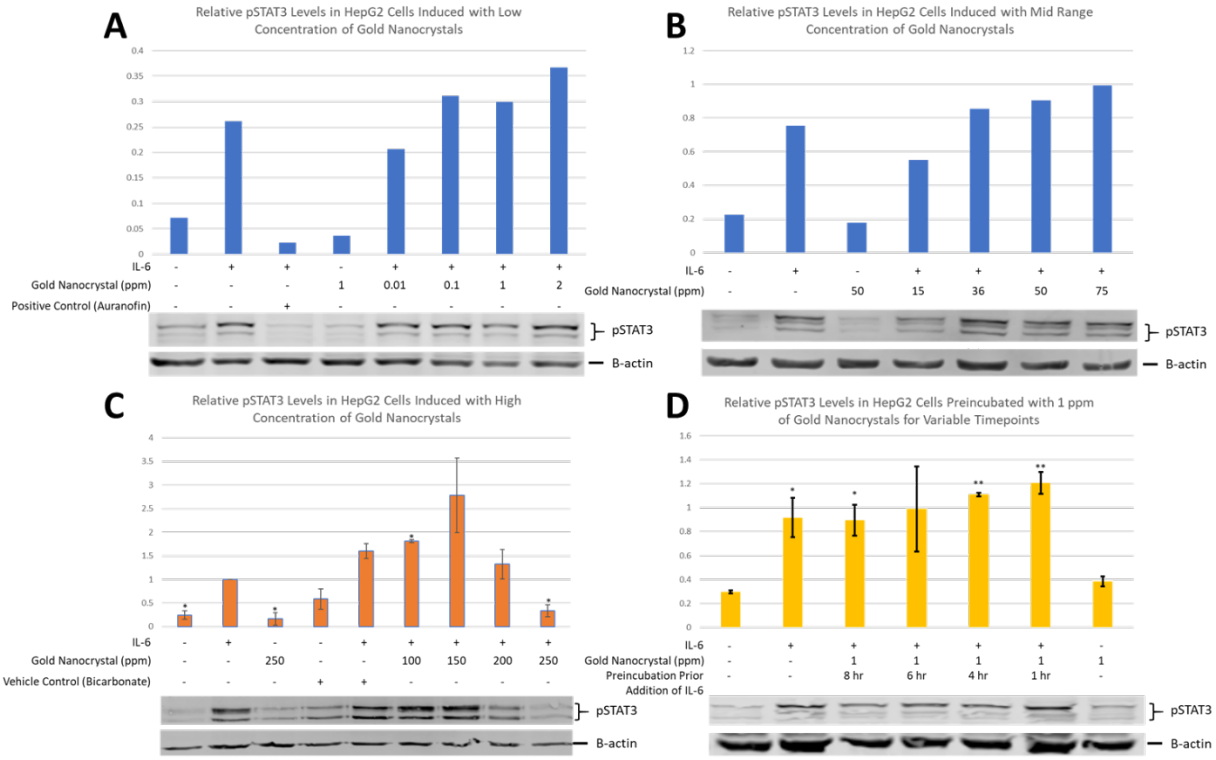

*Figure 12: Inhibition of STAT3 to pSTAT3 with Gold Nanocrystals. IL-6 was using to induce inflammation and the phosphorylation of STAT3 in HepG2 Cells while being treated with varying concentrations of gold nanocrystals. **A-D** show western blots and quantifications. Blue graphs indicate only one replicate was used, orange indicates two replicates were used, and yellow indicates three replicates were used. * p-value <0.05, ** p-value <0.01 **A:**Low gold nanocrystals concentration 0.01 -2 ppm. **B:** Midrange gold nanocrystals concentration 15-75 ppm. **C:** High gold nanocrystals concentration 100-250 ppm. **D:** Preincubation time course of HepG2 cells with gold nanocrystals before addition of IL-6 1 hour to 8 hours.*

Discussion

The gold nanocrystals were able to significantly inhibit the phosphorylation of STAT3 at high concentrations of 250 ppm. Unfortunately, in data shared with us by the creators of the gold nanocrystals we were using, the maximum physiological level of nanocrystals obtained in mice was 1 ppm. Because of this data, we concluded that physiologically obtainable levels of the gold nanocrystals would not serve as an effective inhibitor of Jak/Stat3 inflammation in the model of liver inflammation tested here.

We included an Auranofin control in figure 12A showing that Auranofin effectively inhibits the phosphorylation of STAT3 at small concentrations. It appears that the small organic nature of Auranofin, as well as its gold composition, is necessary for it to be therapeutically active. The gold nanocrystals we used are composed of approximately 68,000 gold atoms[31] with a molecular weight of 13,394 kDa, while Auranofin only has one gold atom with an organic scaffold as a molecular weight of 0.679 kDa. This larger difference in size could explain the different abilities of these gold nanocrystals and Auranofin to inhibit STAT3 phosphorylation.

While the gold nanocrystal's size seems to set it apart from small gold medications, it would still be interesting to probe other inflammation-related pathways that gold drugs have targeted. Aurothiomalate is another gold-based drug used to treat Rheumatoid arthritis by increasing MAPK phosphatase 1 expression.[46] Future work could investigate the effects that gold nanocrystals have on this MAPK phosphatase or other inflammatory pathways affected by other gold-based medications. It is interesting to note that the gold nanocrystals, Auranofin, and Aurothiomalate exhibit their therapeutic activity in autoimmune diseases (multiple sclerosis and Rheumatoid arthritis). Perhaps there is still a yet undiscovered link between gold treatments and autoimmune diseases.

CHAPTER 4: Effects of Gold Nanocrystals on Nrf2 Activation

Introduction

To continue probing the biological effects of gold nanocrystals, we turned to a biological pathway known to be affected by small gold nanoparticles: the Nrf2 pathway. Nuclear factor erythroid 2-related factor 2 (Nrf2) is the master regulator of the antioxidant response elements.[47] In a typical oxidative environment, Kelch-like-EH-associated protein 1 (KEAP1) induces the ubiquitylation and degradation of Nrf2 via the proteasome in the cytoplasm before it can reach the nucleus. When oxidative stress becomes high, an intracellular disulfide bridge is formed in KEAP-1, causing a 'kink' to form in the protein preventing it from bonding with Nrf2.[48,49] Nrf2 is then free to travel to the nucleus and act as a transcription factor upregulating proteins like Heme Oxygenase-1 (HO-1),[49,50] NAD(P)H quinone oxidoreductase 1 (Nqo1),[51] Sulfiredoxin 1,[52] glutathione S-transferase,[53] UDP-glucuronosyltransferase,[54] and other proteins involved in protecting against oxidative stress (Figure 13).

Nrf2 activation helps fight against harmful oxidative agents and is mainly cited for its potential role in cancer protection as well as improve conditions for other diseases.[55,56] That being said, there is some controversy in the field that Nrf2 may not be beneficial in every circumstance. Nrf2 has been implicated in the pathology of some cancers, in which its activation helps cancer cells survive and proliferate.[57] It appears that Nrf2 may be helpful or deleterious depending on the case, but that for most healthy individuals Nrf2 activation appears to be a beneficial thing.[58] Because of this fact, many papers have published potential activators of Nrf2 that could be beneficial health supplements.[59–63]

In a 2015 paper, Lai et al. found that uncapped, spherical, gold nanoparticles 3-5 nm in diameter were capable of inducing the expression of HO-1, a target of Nrf2.[64] They discovered

that this effect could only be disrupted by the presence of thiolated small molecules known to bind to gold surfaces. In this study, they also found the gold nanoparticles did not produce reactive oxygen species or induce ER stress. This led the authors to believe that these gold nanoparticles did not have a toxic oxidative effect on tissue culture cells but could have a beneficial effect by activating antioxidant response genes.[64] Additionally, Auranofin the gold drug is a known activator of Nrf2.[65]

Because other gold nanoparticles and gold medications have been associated with Nrf2 activation, we hypothesized that gold nanocrystals would also be a good activator of Nrf2 because of its known ability to oxidize NADH to NAD^+. We hypothesized that gold nanocrystals would be able to oxidize KEAP1, thereby activating Nrf2. To test this, we treated HepG2 liver cell tissue culture with varying concentrations of gold nanocrystal and then monitored the cell lysates for

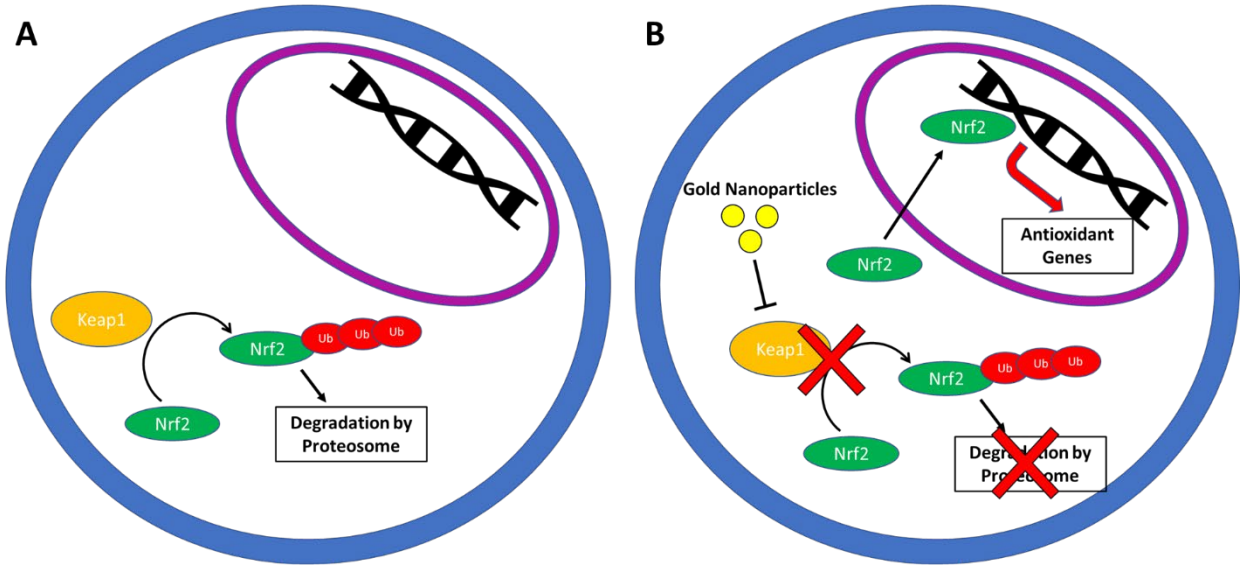

*Figure 13: Nrf2 Antioxidant Defense Pathway: **A:** Under normal conditions, Keap1 ubiquitinylates Nrf2 causing it to be degraded by the proteosome. **B:** When an oxidative inducer such as small gold nanoparticles are added to a cell, Keap1 is inhibited and Nrf2 translocates to the nucleus. Once in the nucleus Nrf2 acts as a transcription factor and upregulates beneficial antioxidant gene expression.*

increases in HO-1, a protein product upregulated by Nrf2 activation.

Experimental

HepG2 Cell Culture and Treatment

HepG2 liver epithelial cells were cultured at 37 °C with Eagles Minimum Essential Medium (EMEM) supplemented with 10% FBS and 100 units/mL penicillin. Cells were maintained between 50% - 80% confluent and split at a 1:5 ratio when 80% - 90% confluent at low passage number (<20 passages). Cells were split with 0.05% trypsin until adherence was lost, and cells were isolated by centrifugation at 1000 RPM for 4 minutes. The supernatant was discarded, and cells were resuspended in supplemented EMEM media. Resuspended cells were plated at 1/5 of their original concentration.

For treatment, cells were split and plated at a density of $5x10^6$ cells/mL and grown overnight. The following day cells were induced with differing concentrations of gold nanocrystal or one of three positive controls known to activate the Nrf2 pathway: 10 µm 2-Trifluoromethyl-2'-methoxychalcone (Cayman Chemical #11881), 20 µm 3H-1,2-Dithiole-3-thione (Abcam #AB141925), and 10 µm Sulforaphane (Sigma Aldrich #S4441). Treated cells were incubated at 37 °C for 6 or 12 hours, as noted.

Lysis

After treatment, media was removed, and cells were washed three times in sterile PBS buffer while on ice. Cells were isolated by centrifugation at 1000 rpm at 4 °C for 4 minutes, followed by the removal of PBS supernatant. Cells were lysed by adding 200 µL RIPA buffer (150 mM NaCl, 50 mM Tris-Base, 0.5% Sodium Deoxycholate, 0.1% SDS, 1% Triton-X, 1 aliquot of HALT (Thermo Fisher catalog#78430) protease inhibitor cocktail/10 mL RIPA) and then flash-frozen in liquid nitrogen followed by immediate thawing in a 37 °C water bath. After thawing, the

lysate was pipetted up and down 10x in a 22-gauge needle to shear the DNA. Samples were then centrifugated at 14,000 RCF for 30 minutes at 4 °C to pellet out the DNA.

Western Blotting

The amount of protein in each cell lysate was quantified using the protocol developed by Lowry et al.[45] Twelve bovine serum albumin (BSA) standards between 0 and 55 µg/mL were run in duplicate and used to quantify each sample that was run in triplicate. 25 µg of each sample was combined with 5 µL of 5X loading dye (250 mM Tris-HCl pH 6.8, 10% SDS, 30% glycerol, 5% β-Mercaptoethanol, 0.02% Bromophenol Blue) and heated at 95 °C for 5 minutes. Samples were then centrifugated briefly and then added to separate with a protein MW standard ladder (GoldBio #P007-500) lanes in a 1.5 cm 5% acrylamide stacking gel on top of a 12% acrylamide Tris-SDS separating gel submerged in SDS-PAGE running buffer (25 mM Tris-Base pH 7.6, 200 mM Glycine, 1% SDS). Loaded gels were run at 150 V for 60 minutes or until dye had reached the end of the gel.

When SDS-PAGE gels had finished running, the gel was removed, rinsed with distilled water, and placed on a nitrocellulose membrane, and sandwiched between two pieces of filter paper and two sponges in a western blot cassette submerged in chilled transfer buffer (25 mM Tris-Base pH 7.6, 200 mM Glycine, 20% methanol). The western blot cassette was placed in a transfer tank filled with transfer buffer and chilled with ice. The protein was transferred from the gel to the nitrocellulose membrane at 0.25 Amps (constant current) for 90 minutes.

When the transfer was complete, membranes were removed, rinsed with TBS buffer (10 mM Tris-Base pH 7.6, 150 mM NaCl), and then dried for 15 minutes. Once dried, the membranes were rehydrated with distilled water and blocked in 5 mL of blocking buffer (10 mM Tris-Base

pH 7.6, 150 mM NaCl, 5% powdered milk, 0.1% tween-20) shaking for 1 hour. At the end of 1 hour, 5 µL of anti-Heme Oxygenase-1 (Cell Signaling Rabbit pAB #70081) and 5 µL of anti-β-actin (Cell Signaling Mouse mAB #3700) were added to the blocking solution and incubated at 4 °C shaking overnight. The next day the antibody solution was removed, and the blot was washed 3x for five minutes with TBS-T (10 mM Tris-Base pH 7.6, 150 mM NaCl, 0.1% tween-20). After washes, 5 mL of blocking buffer with 1 µL of anti-rabbit (Licor Donkey #926-32213 800 nm fluorescence) and 1 µL of anti-mouse (Licor Donkey #926-68072 680 nm fluorescence) secondary antibodies conjugated to fluorescent probes was added to the blots to incubate for 1 hour. At the end of one hour, antibodies were removed, and the blots were rinsed three times with TBS buffer.

Western Blot Data Analysis

Blots were imaged on the LI-COR Odyssey® CLx scanner scanning for fluorescence at 680 nm and 800 nm. Images were processed and quantified using ImageStudio™ Lite software. Pixel intensity was calculated for bands of interest. One single Heme Oxygenase-1 band at 34.6 kDa was quantified for each lane on the 800 nm channel, and a single β-actin band at 42 kDa was quantified on the 680 nm channel in each lane. To normalize samples, the HO-1 intensity was divided by the β-actin intensity for every lane. For replicates across gels, each normalized intensity was divided by the normalized intensity of the wildtype negative control. Averages and standard deviations were calculated for each sample across replicates. One-tailed heteroscedastic T-tests were calculated against the wildtype negative control sample. P-values less than 0.05 were considered significant.

Results

Effect of Gold Nanocrystals on Nrf2 Induction

We hypothesized that the larger (13-15 nm) gold nanocrystals would have a similar effect as the 3-5 nm spherical gold nanoparticles tested by Lai et al.[64] We incubated HepG2 cells with various concentrations of the gold nanocrystals and western blotted for heme oxygenase-1 (HO-1), which Nrf2 upregulates to test this hypothesis. The results from these blots are shown below in figure 14. In these experiments, we used three different Nrf2 activators as a positive control, Sulforaphane (SFN), 2-Trifluoromethyl-2'-methoxychalcone (2T2M), and 3H-1,2-Dithiole-3-thione (D3T). During a 6-hour induction, the best and most consistent activator was 2T2M, and those results are shown in 14a. None of the gold nanocrystal treatments ranging from 0.01 to 2 ppm in concentration affected HO-1 levels during that 6 hours. To be sure of this we tested the same concentrations of the gold nanocrystals during a 12-hour induction to make sure that it was not a slow induction of Nrf2. However, even during the 12-hour induction, we observed no changes in HO-1 levels (figure 14B).

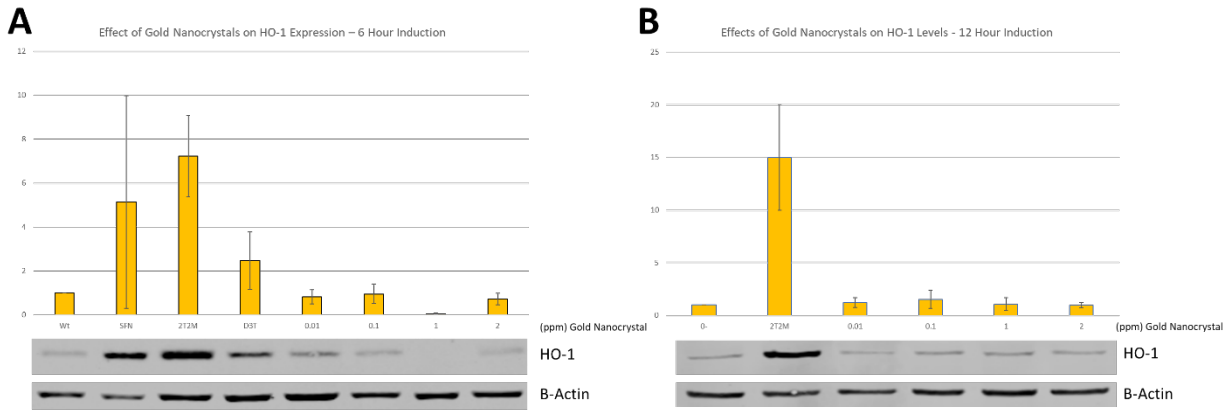

Figure 14: Induction of Heme Oxygenase-1 with Gold Nanocrystals. HepG2 cells were treated with known inducers of Nrf2 or varying concentrations of gold nanocrystals, and the amount of HO-1 was measured as a readout of activation. ***A-B s****hows western blots and quantifications. Yellow graphs indicate that three replicates were used. * p-value <0.05.* ***A:*** *6-hour induction of HepG2 cells with controls and gold nanocrystals.* ***B:*** *12-hour induction of HepG2 cells with control and gold nanocrystals..*

Discussion

Our experiments show that physiologically relevant levels of the gold nanocrystals (around 1 ppm) are not sufficient to stimulate the Nrf2 pathway to produce HO-1. This was a surprising finding since similar gold nanoparticles have previously shown to be excellent activators of Nrf2.[64] A shortcoming in our experiment was that we didn't have access to the same gold nanoparticles tested by Lai et al. to be used as a positive control. It would have been good to see if our experimental conditions were sufficient to confirm their results and validate our own.

One key difference between the nanoparticles tested by Lai et al. and the gold nanocrystals we used is size. Their nanoparticles were 3-5 nm in diameter while the gold nanocrystals we used have a diameter around 15 nm in diameter. Previous studies have found that small gold nanoparticles 1.4-1.5 nm in diameter to be toxic in vitro and some animal models.[66–68] While it has been shown that 5 nm gold nanoparticles are relatively safe[68] it is possible that the smaller-sized nanoparticles are more catalytic, or that a greater concentration can enter cells and interact on molecular scales. It is possible that as nanoparticles get larger, their ability to interact with cells on a molecular level is slowly lost. This could explain why the 5 nm gold nanoparticles were able to activate Nrf2 and the gold nanocrystals were not.

In the future, it would be interesting to observe the activation of Nrf2 with a wide array of gold nanoparticles and nanocrystals differing in size and shape. There could be interesting treads in Nrf2 activation related to size and shape. Given more time, I would like to perform an extensive characterization of all different sizes and shapes of nanoparticles to determine what factors make them good activators of Nrf2.

CHAPTER 5: Isolation and Identification of the Protein Corona of Gold Nanocrystals

Introduction

Knowing any drug's direct interactors is essential to understanding its mechanism. This is especially true for nanoparticles due to what is known by those in material science as 'biofouling'.[69] When nanoparticles are placed in biological solutions, a protein 'corona' spontaneously forms on the nanoparticle's surface. This protein corona affects cellular internalization, covers up catalytic surfaces, and determines the nanoparticle's biological identity.[70–72] Learning the identity and dynamics of a nanoparticle's protein corona is essential to understanding how it will function *in vivo*. To our knowledge, a protein corona has not been characterized for gold nanocrystals.

The protein corona is known to be dynamic, with different coronas being formed in different tissues and settings.[35] Understanding the protein corona of gold nanocrystals in different tissues would allow us to see what proteins are near the nanocrystal's catalytic surface and generate a new hypothesis about their mode of action. Additionally, understanding the protein corona of gold nanocrystals could help us understand their disposition while traveling through a living organism and potential cell types with which it may preferentially interact. This may be especially important since it is known that the protein corona sometimes disguises nanoparticles so they can gain entry into specific cell types.[73]

Our work in this chapter characterizes a method for isolating the protein corona from gold nanocrystals in a way that can directly prepare the protein samples for mass spectrometry and proteomic analysis. It also offers a preliminary characterization of the protein corona of gold nanocrystals in fetal bovine serum (FBS).

Experimental

Setup and Controls

The protocol for isolating the gold nanocrystal's protein corona was inspired by several other papers that performed proteomic analysis on the protein corona of other nanoparticles.[74–78] One key difference between the protocols in these papers and the protocol presented here is that we did not use an SDS-PAGE gel to separate proteins prior to LC-MS^2. Instead, by using guanidine HCl and TCEP as elution agents, we were able to feed our protocol for isolating the protein corona to a spin-filter proteomic mass spec prep protocol adapted from Wis´niewski et al.[79] This protocol allowed us to prepare the protein corona for mass spectrometry using well-known methods without having to perform any complex buffer exchanges.

The gold nanocrystal's FBS protein corona was formed and isolated by incubating the nanoparticles in FBS and then isolating the nanoparticle with its protein corona by centrifuging and removing the supernatant. The nanocrystal-PC complex was then washed by resuspending it in PBS, centrifuging, and removing the supernatant. This washing process was repeated three times. After the last centrifugation, the nanocrystals were resuspended in a reducing and denaturing agent that would reduce any gold thiol bonds and remove non-specific protein-gold interaction. This solution was heated to assist in the denaturation. After causing the protein corona and the gold nanocrystals to dissociate, the nanoparticles were separated from the solution by centrifugation. The supernatant was removed and its protein content quantified. These samples were then trypsin digested and prepared for mass spec. When ready, samples were run on LC-MS^2 on an Orbitrap mass spectrometer. Peak assignments were made using PEAKS mass spec software. This process is shown in figure 15.

For every FBS-gold nanocrystal sample run, a no-gold-control was also included. This no-gold-control was a sample identical to the FBS- gold nanocrystal, but with no nanocrystals, only FBS was included. These controls were treated the same as the nanocrystal samples and run using LC-MS^2 as well. These no-gold-controls allowed us to control for our washing steps and provide a baseline from which we could calculate fold change from control to an actual sample.

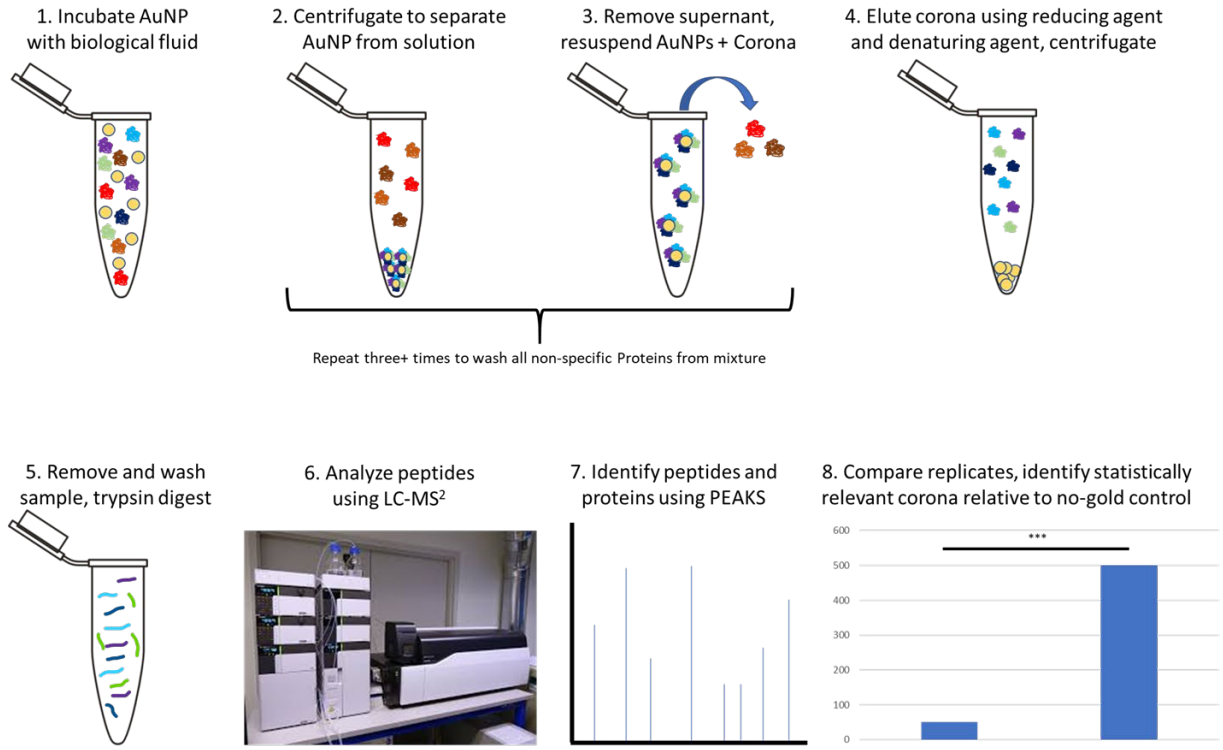

Figure 15: Experimental Workflow to Isolate and Analyze the Protein Corona of Gold Nanocrystals. Gold nanocrystals are incubated with a biological fluid allowing a protein corona to form. This nanoparticle-corona complex is isolated via centrifugation and washed to remove excess protein. Once washed, the protein corona is isolated from the gold by addition of denaturing and reducing agents. The isolated protein corona is then digested and analyzed using LC-MS^2. PEAKS software is used to make peptide assignments from which fold changes and statistical significance can be calculated.

Forming and Isolating an FBS Protein Corona on Gold Nanocrystals

1.6 mL of 500 ppm gold nanocrystals was incubated with 0.4 mL of FBS (Corning #35-010-CV) in three 15 mL conical vials. For the no-gold-controls, 1.6 mL of 6 mM sodium bicarbonate (the vehicle of the gold nanocrystals) was combined with 0.4 mL of FBS in three 15

mL conical vials. Both samples and controls were incubated in a 37 °C water bath for 1.5 hours to encourage protein corona formation. After incubation, samples were centrifugated at 20,000 G for 1 hour at 4 °C (to maintain protein corona interactions). The FBS supernatant was carefully removed using a pipette and leaving only a small layer of liquid over the nanoparticle pellet. For the no gold control, approximately 20 µL of liquid was left at the bottom of the tube. Each sample was then resuspended in 1 mL of 7 mM sodium bicarbonate, mixed well, and then centrifugated at 20,000 G for 1 hour. The addition of sodium bicarbonate, centrifugation, and subsequent removal of supernatant was repeated a total of three times. After the last centrifugation, the wash supernatant was removed and the samples were resuspended in 200 µL of 6M Guanidine-HCl, 100 mM Tris-HCl pH 8.5, 50 mM tris(2-carboxyethyl)phosphine (TCEP). Once resuspended, samples and controls were heated to 90 °C for 30 minutes. At the end of 30 minutes, the samples and controls were centrifugated at 20,000 G for 1 hour at 25 °C. When finished the supernatant was removed taking care not to disturb the gold pellet. This supernatant was used in further analysis.

Protein Quantification and Preparation for Mass Spectrometry

The amount of protein in each supernatant was determined using a 96-well Bradford assay (Sigma Aldrich #B6916). After protein quantification 200 mM chloroacetamide (CAM) was added to each sample so that the final CAM concentration was 40 mM; this solution was heated at 90 °C for 10 minutes. At this point, each of the three replicates was combined together (gold nanocrystal PC with gold nanocrystals PC, no-gold-control with no-gold control) to obtain enough protein for mass spectrometric analysis.

The combined sample and the combined control were added to a 30,000 kDa molecular weight cutoff spin filter and spun at 14,000 G for 20 minutes, after which the flow-through was

discarded. These filters were washed two times with 6 M Guanidine HCl, and three times with mass spec wash buffer (5 mM ammonium bicarbonate pH 8, 10% v/v acetonitrile), each time spinning the samples at 14,000 G for 10 minutes and discarding the flow-through. After these washes, the sample was resuspended to 1 µg/µL protein concentration in mass spec wash buffer, the control was resuspended in the same volume as the sample. Trypsin protease (New England Biolabs #P8101S) was added to a 1:50 trypsin:protein ratio and left to shake overnight at 37 °C. At the end of this incubation period, phenylmethylsulfonyl fluoride (PMSF) was added to a final concentration of 1 mM to stop the trypsin digest. This digested solution was spun on its spin filter at 14,000 G for 20 minutes, the filtrate was collected and put in a mass spec vial, the filter was washed with 100 µL mass spec wash buffer and centrifugated as before, this filtrate was added to the original flow through in the mass spec vial. All samples were dehydrated for 2 hours on a SpeedVac system and stored in the -80 °C freezer.

Liquid Chromatography and Mass Spectrometry

Only one gold nanocrystal protein corona replicate and one no-gold-control replicate were submitted for mass spectrometry. Samples were run by the Fritz B. Burns Biological Mass spectrometry facility. Both samples were resuspended in mass spec buffer A (0.1% formic acid in optima water) to 1 µg/µL for the gold nanocrystal PC sample, the same volume was used to resuspend the control. 6 µL of both the sample and control were injected on an EASY-nLC liquid chromatography (LC) unit (Thermo Fisher) online with an Orbitrap Fusion Lumos Tribrid Mass Spectrometer (Thermo Fisher). A rapid separation LC (RSLC) column (EASY-spray column pepMap ® RSLC, C18, 2 µM, 100 Å, 75 µM × 15 cm) was used to separate peptides. Mass spec buffers A (0.1% formic acid in optima water) and B (optima water and 0.1% formic acid in 80%

acetonitrile) served as the mobile phase for LC. The peptides were eluted at 300 nL/min with the following gradients over 2 h: 5–22% B for 85 min; 22–32% B for 15 min; 32–95% B for 10 min; and 95% for 10 min. Nano-spray ionization was used to introduce ions to the Orbitrap.

Peptide sequence data was acquired using 3-second scan cycles in data dependent acquisition (DDA) mode. The Orbitrap resolution was set to 120,000 with a scan range between 375 and 1700 m/z. The intensity threshold was set to 5e3 with a maximum injection time of 50 ms. Peptides with charge states of 2–6 were selected from the top abundant peaks by the quadrupole for high-energy collisional dissociation (HCD with normalized energy 30, activation time 10 ms) MS/MS, and the fragment ions were detected in the linear ion trap with target AGC value of 1e4 and a dynamic maximum injection time. The dynamic exclusion time was set at 60 s. Precursor ions with ambiguous charge states were not fragmented.

Data Analysis

PEAKS software (version 8.5) was used to make peak assignments on the mass spec data for further quantification. The Swiss-Prot *Bos taurus* database was used to search the mass spectra and make assignments based on homology matches. In brief, the variables for the search were: fixed carbamidomethylation and variable methionine oxidation/pyroglutamate from glutamine, fragment ion tolerance: 0.5, max number of PTM's: 3, de novo score(%) threshold: 15, peptide hit threshold: (-10logP): 30.

Once peaks had been assigned the top 118 proteins found in the gold nanocrystal's protein corona but not in the no-gold-control were submitted to the Database for Annotation, Visualization, and Integrated Discovery (DAVID) online server against a *Bos taurus* background. These 118 proteins were classified using COG Ontology, Up Keywords, Up Seq Feature, GoTerm

BP Direct, GoTerm CC Direct, GoTerm MF Direct, KEGG Pathway, InterPro, PIR Superfamily, and Smart annotation lists. These were used to create functional annotation clustering under high stringency from the 118 proteins submitted from which the top three clusterings were reported in the results section.

SDS-PAGE Analysis of the Protein Corona Isolation

A separate experimental set of gold nanocrystals and the no-gold-control were incubated and isolated as before, only 200 µL of 5X loading dye (250 mM Tris-HCl pH 6.8, 10% SDS, 30% glycerol, 5% β-Mercaptoethanol, 0.02% Bromophenol Blue) was added to elute the protein corona from the nanoparticles while being heated at 90 °C for 30 minutes. In addition to the final elution from the gold nanocrystals and the no-gold-control, 50 µL samples were taken from the original FBS supernatant and each of the washes to assess isolation efficiency. To each of these additional samples, 5 µL of 5x loading dye was added and samples were heated at 90 °C for 10 minutes. All samples were then centrifugated briefly and 50 µL were added with a protein MW standard ladder (GoldBio #P007-500) to separate lanes in a 1.5 cm 5% acrylamide stacking gel on top of a 12% acrylamide Tris-SDS separating gel submerged in SDS-PAGE running buffer (25 mM Tris-Base pH 7.6, 200 mM Glycine, 1% SDS). Loaded gels were run at 150 V for 60 minutes or until dye had reached the end of the gel.

When SDS-PAGE gels had finished running, the gel was removed, rinsed with distilled, water, and then soaked in destain buffer 1 (50% methanol and 10% glacial acetic acid) for 30 minutes to fix the gel. This buffer was removed and Coomassie blue stain (0.1% Coomassie Brilliant Blue R-250, 50% methanol, and 10% glacial acetic acid) was added, microwaved on high for 15 seconds, then allowed to stain for 30 minutes. Coomassie stain was then removed, the gel

was rinsed with water, destain buffer 1 was added, and the gel was microwaved on high for 15 seconds. Destain buffer 1 was immediately discarded, and destain buffer 2 (40% methanol and 10% glacial acetic acid) was added to the gel and microwaved for 15 seconds. This mixture was allowed to shake overnight with a Kimwipe until gel had destained and bands were visible. Gels were imaged on the LI-COR Odyssey® CLx scanner scanning at 680 nm and 800 nm. Images were processed using ImageStudio™ Lite software.

Lowry Analysis of Protein Corona Isolation

To confirm the efficiency of protein corona isolation, a protein quantification based on the technique by Lowry et al.[45] was performed in triplicate on the FBS supernatant, the ammonium bicarbonate washes, and elution that had been washed with mass spec wash buffer from the gold nanocrystals protein corona isolation. Twelve bovine serum albumin (BSA) standards between 0 and 55 µg/mL were used to quantify the sample. One-tailed heteroscedastic T-tests were calculated for the absorbance at 750 nm between the 0 µg negative control and all other samples. P-values less than 0.05 were considered significant.

Results

Isolation of the Gold Nanocrystal FBS Protein Corona

To confirm our ability to isolate the protein corona from gold nanocrystals, we ran samples from the original FBS supernatant, the wash steps, and the final elution of the protein corona on an SDS-PAGE acrylamide gel and stained for total protein using Coomassie blue. We repeated this process on the no-gold-control as well. The resulting SDS-PAGE gels are shown in figure 16A-B. In both gels, many intense protein bands are evident in the FBS supernatant lane with the

highest abundance protein between 63 and 75 kDa (bovine serum albumin MW=66kDa). All protein bands decreased in intensity for each wash lane until only a faint band was observed above 63 kDa (most likely BSA) in wash four. In figure 16A, the no-gold-control elutions show only faint bands around 63 kDa. In figure 16B, the gold nanocrystal protein corona elutions show a very specific banding pattern. These figures together show that while not perfect, our isolation seems to work very effectively to obtain the protein corona.

To add additional evidence to our ability to isolate the gold nanocrystal's protein corona we use a Lowry assay to quantify the protein in each of the purification steps from the same

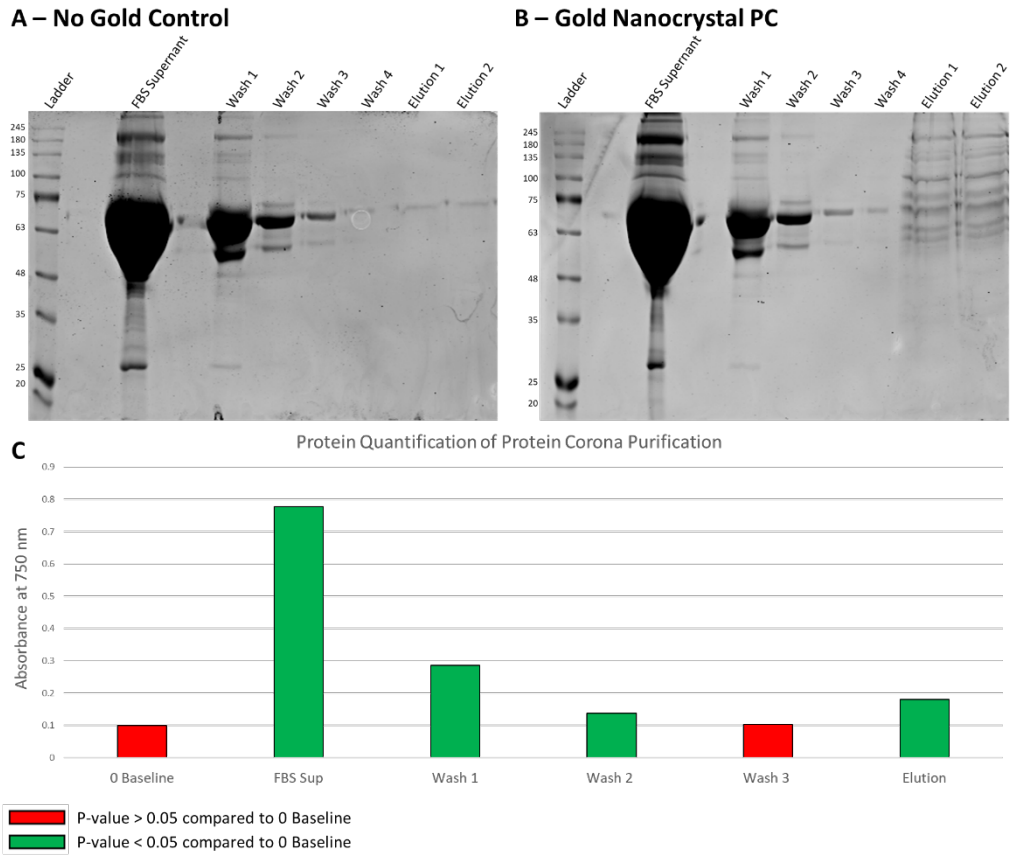

Figure 16: Isolation of the Protein Corona of Gold Nanocrystals in FBS. The gold nanocrystal's FBS protein corona was isolated by centrifugation and 4 PBS washes. Guanidine-HCl and TCEP were used to remove the protein corona. ***A:*** *SDS-PAGE gel stained with Coomassie blue of no gold control washes and elutions, almost no protein is seen in these elutions.* ***B:*** *SDS-PAGE gel stained with Coomassie blue of gold nanocrystal washes and elutions, a very specific protein pattern is seen in the elutions of the protein corona. MW BSA =66 kDa.* ***C:*** *Lowry assay showing the quantification of protein in each of the washes and elution of the gold nanocrystal protein corona. Green bars were significantly different (p-value<0.05) than the 0 baseline, while red bars were not significantly different (p-value>0.05)*

purification in triplicate and calculated statistical significance between samples. These results are shown in figure 16C. Decreased total levels of protein are observed until wash 3 when the absorbance readout is statistically indistinguishable from the negative control. The elution then appears to shoot back up and is statistically different from the zero-baseline showing that our elution strategy is effective.

Mass Spectrometry and Proteomic Analysis

Due to time and reagent constraints, only one gold nanocrystal protein corona replicate and one no-gold-control replicate were submitted for LC-MS^2. Because of this, no statistical significance could be calculated for the resulting data. That being said, I chose to analyze and present this data as a preliminary set of results. This data may not be accurate because no statistical significance was calculated, but it may serve as a starting point for additional studies probing the protein corona of gold nanocrystals.

The mass spec results indicated that 445 proteins had been identified in the gold nanocrystal's protein corona and 352 had been identified in the no-gold-control. Of those proteins identified, 118 were unique to the gold nanocrystal protein corona, 25 were unique to the no-gold-control, and 327 were shared between the two groups (figure 17A). Because I couldn't calculate statistical significance, I chose to only analyze the 118 unique proteins found in the gold nanocrystal's protein corona. I submitted these proteins to the Database for Annotation, Visualization, and Integrated Discovery (DAVID) online to classify the proteins into functional groups and determine what commonalities they may have (figure 17B). Under a high stringency classification, three clusters were made with an enrichment score above two. The top cluster with an enrichment score of 5.56 included secreted signaling peptides rich in disulfide bonds. The

second cluster had an enrichment score of 2.97 and included EF-hand calcium-binding proteins. The third cluster had an enrichment score of 2.24 and was comprised of cysteine proteases. Both cluster 1 and cluster 3 include proteins rich in cysteine thiol groups which are known to form covalent bonds to gold surfaces. These could prove to be real interactions that will need to be monitored in future experiments. Cluster 2 consisted of proteins containing a calcium-binding EF-

A

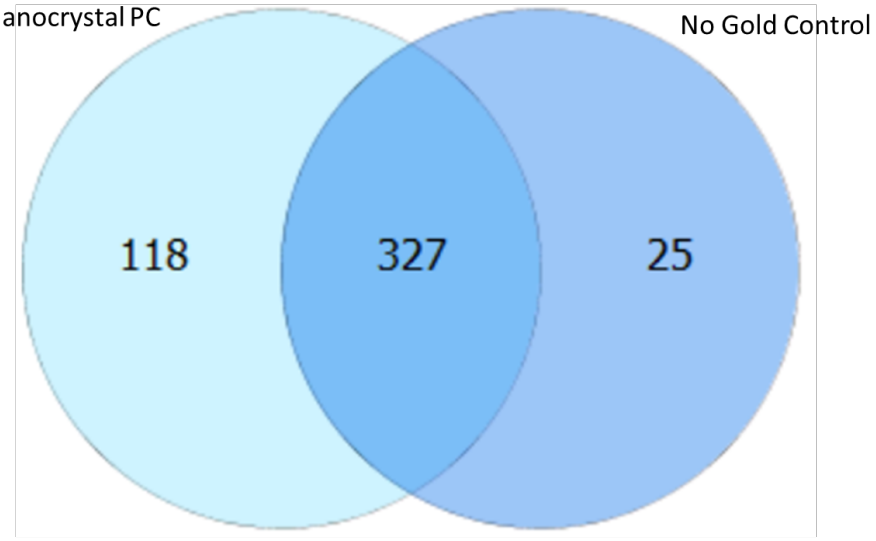

B

Annotation Cluster 1 Enrichment Score: 5.558322373397349

Category	Term	Count	%	PValue	Benjamini	FDR
UP_KEYWORDS	Secreted	29	26.12612613	2.86E-13	1.37E-11	1.12E-11
UP_KEYWORDS	Disulfide bond	31	27.92792793	3.83E-08	9.15E-07	7.48E-07
UP_SEQ_FEATURE	disulfide bond	27	24.32432432	0.001100562	0.432517671	0.432517671
UP_KEYWORDS	Signal	30	27.02702703	0.00307712	0.026714994	0.021819576
UP_SEQ_FEATURE	signal peptide	29	26.12612613	0.004343889	0.496289308	0.496289308

Annotation Cluster 2 Enrichment Score: 2.9733189127793467

Category	Term	Count	%	PValue	Benjamini	FDR
INTERPRO	IPR002048:EF-hand domain	8	7.207207207	3.07E-04	0.056770346	0.056445944
INTERPRO	IPR018247:EF-Hand 1, calcium-binding site	7	6.306306306	5.18E-04	0.060486693	0.060141055
INTERPRO	IPR011992:EF-hand-like domain	8	7.207207207	0.001060162	0.092764183	0.092234102
UP_SEQ_FEATURE	domain:EF-hand 2	7	6.306306306	0.002839284	0.432517671	0.432517671
UP_SEQ_FEATURE	domain:EF-hand 1	7	6.306306306	0.002839284	0.432517671	0.432517671

Annotation Cluster 3 Enrichment Score: 2.2364689553281893

Category	Term	Count	%	PValue	Benjamini	FDR
INTERPRO	IPR000169:Cysteine peptidase, cysteine active site	4	3.603603604	3.24E-04	0.056770346	0.056445944
UP_KEYWORDS	Thiol protease	4	3.603603604	0.007913618	0.058134659	0.047481711
GOTERM_CC_DIRECT	GO:0005764~lysosome	4	3.603603604	0.076056185	0.603922126	0.581239605

Figure 17: Data Analysis of 1 Replicate of the Gold Nanocrystal PC and No Gold Control. ***A:*** *PEAKS analysis of mass spectrometry data identified 445 proteins in the gold nanocrystal PC and 352 proteins in the no gold control. 118 proteins were identified in the gold nanocrystal PC that were not found in the no gold control.* ***B:*** *Those 118 proteins were submitted to the Database for Annotation, Visualization, and Integrated Discovery (DAVID), searching for significant clustering patterns against a Bos taurus background. The top three clusters obtained after being searched with high stringency are shown in this table. Cluster 1 included secreted signaling peptides rich in disulfide bonds. Cluster 2 included EF-hand calcium binding domains. Cluster 3 included cysteine proteases.*

hand domain, it is possible that this domain that binds to calcium ions also interacts with a surface composed of gold ions.

Discussion

In this chapter, we confirmed that we can successfully purify and isolate the protein corona of gold nanocrystals. We also obtained preliminary mass spectrometry results of gold nanocrystal's protein corona in FBS, which serves as a model of human serum. Unfortunately, due to limitations in time and reagents, we were only able to characterize one replicate of this protein corona and its control. Because of that, the results obtained could not be analyzed statistically making it difficult to determine which proteins were really present in the protein corona but not in the no-gold-control. Due to this fact, these results cannot be used as a final conclusion as to the composition of the gold nanocrystal's protein corona, but they can be used as a preliminary list from which to pursue future experiments.

These preliminary results identified 118 proteins bound uniquely to the gold nanocrystals while 327 were also found in the no-gold-control. It would be good to increase the number of washes during purification to reduce the number of proteins being identified in the no-gold-control and find out if some of these 327 proteins are also specific to the gold nanocrystal's protein corona.

The results from DAVID clustering indicate that some cysteine and EF-hand containing proteins from FBS tend to associate with gold nanocrystals and form the protein corona. These results were searched against a general *Bos taurus* background. A better background would be the serum proteome from FBS that could distinguish how enriched these proteins are specifically in serum. Running an FBS control sample on LC-MS^2 to serve as a background will be a necessary addition to our experimental methods to obtain stronger results. In the future, it would also be very

interesting to not only replicate these results but also to see if this same type of clustering appears in the gold nanocrystal's protein corona in different biological settings, such as in liver or nerve cells.

Future studies could pursue the identity of the gold nanocrystal's protein corona in neurons and oligodendrocytes to determine how the protein corona could be affecting a nanocrystals ability to treat neurodegenerative disease. Another interesting study that could be pursued would be to form a serum corona around the gold nanocrystals and use those to treat neural cells. An analysis of the resulting protein corona (serum+neural) would give a picture of how much the serum corona remains on the nanocrystals after entering a new biological environment (the neuron). Yet another study that could be performed would be to test gold nanocrystal's catalytic efficiency to oxidize NADH to NAD^+ (modeling the experiment done by Robinson et al.)[31] with different protein coronas to determine under what setting the gold nanocrystals displays optimal catalytic activity.

Although this study remains incomplete, the promise of new insights into the mechanism of gold nanocrystals makes the study of its protein corona very promising. The work in this chapter provides a framework by which future protein corona proteomic experiments can be pursued, not only on the gold nanocrystals we tested, but also on other nanoparticles.

REFERENCES

(1) Headache Causes https://www.mayoclinic.org/symptoms/headache/basics/definition/sym-20050800 (accessed Feb 27, 2021).

(2) Pai, M.; Walia, K.; Boehme, C. C. Essential Medicines and Essential Diagnostics: A Package Deal. *Lancet Public Health* **2019**, *4* (10), e492. https://doi.org/10.1016/S2468-2667(19)30165-3.

(3) WHO | Second WHO Model List of Essential In Vitro Diagnostics http://www.who.int/medical_devices/publications/Second_WHO_Model_List_of_Essential_In_Vitro_Diagnostics/en/ (accessed Feb 1, 2021).

(4) WHO | A guide to aid the selection of diagnostic tests http://www.who.int/bulletin/volumes/95/9/16-187468/en/ (accessed Feb 1, 2021). https://doi.org/10.2471/BLT.16.187468.

(5) Gubala, V.; Harris, L. F.; Ricco, A. J.; Tan, M. X.; Williams, D. E. Point of Care Diagnostics: Status and Future. *Anal. Chem.* **2012**, *84* (2), 487–515. https://doi.org/10.1021/ac2030199.

(6) Sun, Y.; Xia, Y. Gold and Silver Nanoparticles: A Class of Chromophores with Colors Tunable in the Range from 400 to 750 Nm. *Analyst* **2003**, *128* (6), 686–691. https://doi.org/10.1039/B212437H.

(7) Jazayeri, M. H.; Amani, H.; Pourfatollah, A. A.; Pazoki-Toroudi, H.; Sedighimoghaddam, B. Various Methods of Gold Nanoparticles (GNPs) Conjugation to Antibodies. *Sens. Bio-Sens. Res.* **2016**, *9*, 17–22. https://doi.org/10.1016/j.sbsr.2016.04.002.

(8) ServiceMay. 22, R. F.; 2020; Pm, 3:35. Coronavirus antigen tests: quick and cheap, but too often wrong? https://www.sciencemag.org/news/2020/05/coronavirus-antigen-tests-quick-and-cheap-too-often-wrong (accessed Feb 2, 2021).

(9) Vandenberg, O.; Martiny, D.; Rochas, O.; van Belkum, A.; Kozlakidis, Z. Considerations for Diagnostic COVID-19 Tests. *Nat. Rev. Microbiol.* **2020**, 1–13. https://doi.org/10.1038/s41579-020-00461-z.

(10) Bobbitt, J. M. Periodate Oxidation of Carbohydrates. In *Advances in Carbohydrate Chemistry*; Wolfrom, M. L., Tipson, R. S., Eds.; Academic Press, 1956; Vol. 11, pp 1–41. https://doi.org/10.1016/S0096-5332(08)60115-0.

(11) Kristiansen, K. A.; Potthast, A.; Christensen, B. E. Periodate Oxidation of Polysaccharides for Modification of Chemical and Physical Properties. *Carbohydr. Res.* **2010**, *345* (10), 1264–1271. https://doi.org/10.1016/j.carres.2010.02.011.

(12) Nikolic, T.; Kostic, M.; Praskalo, J.; Pejic, B.; Petronijevic, Z.; Skundric, P. Sodium Periodate Oxidized Cotton Yarn as Carrier for Immobilization of Trypsin. *Carbohydr. Polym.* **2010**, *82* (3), 976–981. https://doi.org/10.1016/j.carbpol.2010.06.028.

(13) Nikolic, T.; Milanovic, J.; Kramar, A.; Petronijevic, Z.; Milenkovic, L.; Kostic, M. Preparation of Cellulosic Fibers with Biological Activity by Immobilization of Trypsin on Periodate Oxidized Viscose Fibers. *Cellulose* **2014**, *21* (3), 1369–1380. https://doi.org/10.1007/s10570-014-0171-0.

(14) Wang, Q.; Li, C. X.; Fan, X.; Wang, P.; Cui, L. Immobilization of Catalase on Cotton Fabric Oxidized by Sodium Periodate. *Biocatal. Biotransformation* **2008**, *26* (5), 437–443. https://doi.org/10.1080/10242420802335031.

(15) Pejic, B.; Baralic, A. M.; Kojic, Z.; Skundric, P.; Kostic, M. Oxidized Cotton as a Substrate for the Preparation of Hormone-Active Fibers-Characterization, Efficiency and

Biocompatibility. *Fibers Polym.* **2015**, *16* (5), 997–1004. https://doi.org/10.1007/s12221-015-0997-6.
(16) Gurvich, A. E.; Lechtzind, E. V. High Capacity Immunoadsorbents Based on Preparations of Reprecipitated Cellulose. *Mol. Immunol.* **1982**, *19* (4), 637–640. https://doi.org/10.1016/0161-5890(82)90233-4.
(17) Isobe, N.; Lee, D.-S.; Kwon, Y.-J.; Kimura, S.; Kuga, S.; Wada, M.; Kim, U.-J. Immobilization of Protein on Cellulose Hydrogel. *Cellulose* **2011**, *18* (5), 1251. https://doi.org/10.1007/s10570-011-9561-8.
(18) Zhu, X.; Xiong, S.; Zhang, J.; Zhang, X.; Tong, X.; Kong, S. Improving Paper-Based ELISA Performance through Covalent Immobilization of Antibodies. *Sens. Actuators B Chem.* **2018**, *255*, 598–604. https://doi.org/10.1016/j.snb.2017.08.090.
(19) Y, P.; Vv, G.; A, A.; Kh, P. Covalent Binding of Antibodies to Cellulose Paper Discs and Their Applications in Naked-Eye Colorimetric Immunoassays. *J. Vis. Exp. Jove* **2016**, No. 116. https://doi.org/10.3791/54111.
(20) Zhang, X.; Shen, G.; Sun, S.; Shen, Y.; Zhang, C.; Xiao, A. Direct Immobilization of Antibodies on Dialdehyde Cellulose Film for Convenient Construction of an Electrochemical Immunosensor. *Sens. Actuators B Chem.* **2014**, *200*, 304–309. https://doi.org/10.1016/j.snb.2014.04.030.
(21) Alamer, S.; Eissa, S.; Chinnappan, R.; Herron, P.; Zourob, M. Rapid Colorimetric Lactoferrin-Based Sandwich Immunoassay on Cotton Swabs for the Detection of Foodborne Pathogenic Bacteria. *Talanta* **2018**, *185*, 275–280. https://doi.org/10.1016/j.talanta.2018.03.072.
(22) Wittstock, A.; Neumann, B.; Schaefer, A.; Dumbuya, K.; Kübel, C.; Biener, M. M.; Zielasek, V.; Steinrück, H.-P.; Gottfried, J. M.; Biener, J.; Hamza, A.; Bäumer, M. Nanoporous Au: An Unsupported Pure Gold Catalyst? *J. Phys. Chem. C* **2009**, *113* (14), 5593–5600. https://doi.org/10.1021/jp808185v.
(23) Benedek, T. G. The History of Gold Therapy for Tuberculosis. *J. Hist. Med. Allied Sci.* **2004**, *59* (1), 50–89. https://doi.org/10.1093/jhmas/jrg042.
(24) Kean, W. F.; Kean, I. R. L. Clinical Pharmacology of Gold. *Inflammopharmacology* **2008**, *16* (3), 112–125. https://doi.org/10.1007/s10787-007-0021-x.
(25) Bagheri, S.; Yasemi, M.; Safaie-Qamsari, E.; Rashidiani, J.; Abkar, M.; Hassani, M.; Mirhosseini, S. A.; Kooshki, H. Using Gold Nanoparticles in Diagnosis and Treatment of Melanoma Cancer. *Artif. Cells Nanomedicine Biotechnol.* **2018**, *46* (sup1), 462–471. https://doi.org/10.1080/21691401.2018.1430585.
(26) Farooq, M. U.; Novosad, V.; Rozhkova, E. A.; Wali, H.; Ali, A.; Fateh, A. A.; Neogi, P. B.; Neogi, A.; Wang, Z. Gold Nanoparticles-Enabled Efficient Dual Delivery of Anticancer Therapeutics to HeLa Cells. *Sci. Rep.* **2018**, *8* (1), 2907. https://doi.org/10.1038/s41598-018-21331-y.
(27) Tian, L.; Chang, A.; Melancon, M. P. Exploring Gold Nanoparticle Interactions with Proteins and the Tumor Microenvironment in Biological Systems. *Transl. Cancer Res.* **2017**, *6* (Suppl 2), S309–S312. https://doi.org/10.21037/tcr.2017.03.53.
(28) Sztandera, K.; Gorzkiewicz, M.; Klajnert-Maculewicz, B. Gold Nanoparticles in Cancer Treatment. *Mol. Pharm.* **2019**, *16* (1), 1–23. https://doi.org/10.1021/acs.molpharmaceut.8b00810.

(29) Gold–Palladium Core–Shell Nanocrystals with Size and Shape Control Optimized for Catalytic Performance - Henning - 2013 - Angewandte Chemie - Wiley Online Library https://onlinelibrary.wiley.com/doi/full/10.1002/ange.201207824 (accessed Mar 24, 2021).
(30) Pu, Y.; Zhao, Y.; Zheng, P.; Li, M. Elucidating the Growth Mechanism of Plasmonic Gold Nanostars with Tunable Optical and Photothermal Properties. *Inorg. Chem.* **2018**, *57* (14), 8599–8607. https://doi.org/10.1021/acs.inorgchem.8b01354.
(31) Robinson, A. P.; Zhang, J. Z.; Titus, H. E.; Karl, M.; Merzliakov, M.; Dorfman, A. R.; Karlik, S.; Stewart, M. G.; Watt, R. K.; Facer, B. D.; Facer, J. D.; Christian, N. D.; Ho, K. S.; Hotchkin, M. T.; Mortenson, M. G.; Miller, R. H.; Miller, S. D. Nanocatalytic Activity of Clean-Surfaced, Faceted Nanocrystalline Gold Enhances Remyelination in Animal Models of Multiple Sclerosis. *Sci. Rep.* **2020**, *10* (1), 1–16. https://doi.org/10.1038/s41598-020-58709-w.
(32) Nanocrystalline Gold to Treat Remyelination Failure in Chronic Optic Neuropathy In Multiple Sclerosis - Full Text View - ClinicalTrials.gov https://clinicaltrials.gov/ct2/show/NCT03536559 (accessed Aug 12, 2020).
(33) 31P-MRS Imaging to Assess the Effects of CNM-Au8 on Impaired Neuronal Redox State in Parkinson's Disease - Full Text View - ClinicalTrials.gov https://clinicaltrials.gov/ct2/show/NCT03815916 (accessed Aug 12, 2020).
(34) Therapeutic Nanocatalysis to Slow Disease Progression of Amyotrophic Lateral Sclerosis (ALS) - Full Text View - ClinicalTrials.gov https://clinicaltrials.gov/ct2/show/NCT04098406 (accessed Aug 12, 2020).
(35) Lundqvist, M.; Stigler, J.; Cedervall, T.; Berggård, T.; Flanagan, M. B.; Lynch, I.; Elia, G.; Dawson, K. The Evolution of the Protein Corona around Nanoparticles: A Test Study. *ACS Nano* **2011**, *5* (9), 7503–7509. https://doi.org/10.1021/nn202458g.
(36) Bombardier, C.; Ware, J.; Russell, I. J.; Larson, M.; Chalmers, A.; Read, J. L.; Arnold, W.; Bennett, R.; Caldwell, J.; Hench, P. K.; Lages, W.; Liang, M.; Ludivico, C.; Morgan, G. J.; O'Hanlan, M.; Schur, P.; Sheon, R.; Taylor, T.; McNeil, B.; Pauker, S.; Torrance, G.; Thompson, M. Auranofin Therapy and Quality of Life in Patients with Rheumatoid Arthritis. Results of a Multicenter Trial. *Am. J. Med.* **1986**, *81* (4), 565–578. https://doi.org/10.1016/0002-9343(86)90539-5.
(37) Lewis, M. G.; DaFonseca, S.; Chomont, N.; Palamara, A. T.; Tardugno, M.; Mai, A.; Collins, M.; Wagner, W. L.; Yalley-Ogunro, J.; Greenhouse, J.; Chirullo, B.; Norelli, S.; Garaci, E.; Savarino, A. Gold Drug Auranofin Restricts the Viral Reservoir in the Monkey AIDS Model and Induces Containment of Viral Load Following ART Suspension. *AIDS* **2011**, *25* (11), 1347–1356. https://doi.org/10.1097/QAD.0b013e328347bd77.
(38) Harbut, M. B.; Vilchèze, C.; Luo, X.; Hensler, M. E.; Guo, H.; Yang, B.; Chatterjee, A. K.; Nizet, V.; Jacobs, W. R.; Schultz, P. G.; Wang, F. Auranofin Exerts Broad-Spectrum Bactericidal Activities by Targeting Thiol-Redox Homeostasis. *Proc. Natl. Acad. Sci.* **2015**, *112* (14), 4453–4458. https://doi.org/10.1073/pnas.1504022112.
(39) A high-throughput drug screen for Entamoeba histolytica identifies a new lead and target | Nature Medicine https://www.nature.com/articles/nm.2758 (accessed Feb 27, 2021).
(40) Auranofin displays anticancer activity against ovarian cancer cells through FOXO3 activation independent of p53 https://www.spandidos-publications.com/10.3892/ijo.2014.2579 (accessed Feb 27, 2021).
(41) Rothan, H. A.; Stone, S.; Natekar, J.; Kumari, P.; Arora, K.; Kumar, M. The FDA-Approved Gold Drug Auranofin Inhibits Novel Coronavirus (SARS-COV-2) Replication

and Attenuates Inflammation in Human Cells. *Virology* **2020**, *547*, 7–11. https://doi.org/10.1016/j.virol.2020.05.002.
(42) Kim, N.-H.; Lee, M.-Y.; Park, S.-J.; Choi, J.-S.; Oh, M.-K.; Kim, I.-S. Auranofin Blocks Interleukin-6 Signalling by Inhibiting Phosphorylation of JAK1 and STAT3. *Immunology* **2007**, *122* (4), 607–614. https://doi.org/10.1111/j.1365-2567.2007.02679.x.
(43) Aggarwal, B. B.; Kunnumakkara, A. B.; Harikumar, K. B.; Gupta, S. R.; Tharakan, S. T.; Koca, C.; Dey, S.; Sung, B. Signal Transducer and Activator of Transcription-3, Inflammation, and Cancer. *Ann. N. Y. Acad. Sci.* **2009**, *1171*, 59–76. https://doi.org/10.1111/j.1749-6632.2009.04911.x.
(44) Krause, A.; Scaletta, N.; Ji, J.-D.; Ivashkiv, L. B. Rheumatoid Arthritis Synoviocyte Survival Is Dependent on Stat3. *J. Immunol.* **2002**, *169* (11), 6610–6616. https://doi.org/10.4049/jimmunol.169.11.6610.
(45) Lowry, OliverH.; Rosebrough, NiraJ.; Farr, A. L.; Randall, RoseJ. PROTEIN MEASUREMENT WITH THE FOLIN PHENOL REAGENT. *J. Biol. Chem.* **1951**, *193* (1), 265–275. https://doi.org/10.1016/S0021-9258(19)52451-6.
(46) Nieminen, R.; Korhonen, R.; Moilanen, T.; Clark, A. R.; Moilanen, E. Aurothiomalate Inhibits Cyclooxygenase 2, Matrix Metalloproteinase 3, and Interleukin-6 Expression in Chondrocytes by Increasing MAPK Phosphatase 1 Expression and Decreasing P38 Phosphorylation: MAPK Phosphatase 1 as a Novel Target for Antirheumatic Drugs. *Arthritis Rheum.* **2010**, *62* (6), 1650–1659. https://doi.org/10.1002/art.27409.
(47) Nguyen, T.; Nioi, P.; Pickett, C. B. The Nrf2-Antioxidant Response Element Signaling Pathway and Its Activation by Oxidative Stress*. *J. Biol. Chem.* **2009**, *284* (20), 13291–13295. https://doi.org/10.1074/jbc.R900010200.
(48) Itoh, K.; Wakabayashi, N.; Katoh, Y.; Ishii, T.; Igarashi, K.; Engel, J. D.; Yamamoto, M. Keap1 Represses Nuclear Activation of Antioxidant Responsive Elements by Nrf2 through Binding to the Amino-Terminal Neh2 Domain. *Genes Dev.* **1999**, *13* (1), 76–86. https://doi.org/10.1101/gad.13.1.76.
(49) Wasik, U.; Milkiewicz, M.; Kempinska-Podhorodecka, A.; Milkiewicz, P. Protection against Oxidative Stress Mediated by the Nrf2/Keap1 Axis Is Impaired in Primary Biliary Cholangitis. *Sci. Rep.* **2017**, *7* (1), 44769. https://doi.org/10.1038/srep44769.
(50) Loboda, A.; Damulewicz, M.; Pyza, E.; Jozkowicz, A.; Dulak, J. Role of Nrf2/HO-1 System in Development, Oxidative Stress Response and Diseases: An Evolutionarily Conserved Mechanism. *Cell. Mol. Life Sci.* **2016**, *73* (17), 3221–3247. https://doi.org/10.1007/s00018-016-2223-0.
(51) Venugopal, R.; Jaiswal, A. K. Nrf1 and Nrf2 Positively and C-Fos and Fra1 Negatively Regulate the Human Antioxidant Response Element-Mediated Expression of NAD(P)H:Quinone Oxidoreductase1 Gene. *Proc. Natl. Acad. Sci.* **1996**, *93* (25), 14960–14965. https://doi.org/10.1073/pnas.93.25.14960.
(52) Soriano, F. X.; Baxter, P.; Murray, L. M.; Sporn, M. B.; Gillingwater, T. H.; Hardingham, G. E. Transcriptional Regulation of the AP-1 and Nrf2 Target Gene Sulfiredoxin. *Mol. Cells* **2009**, *27* (3), 279–282. https://doi.org/10.1007/s10059-009-0050-y.
(53) Hayes, J. D.; Chanas, S. A.; Henderson, C. J.; McMahon, M.; Sun, C.; Moffat, G. J.; Wolf, C. R.; Yamamoto, M. The Nrf2 Transcription Factor Contributes Both to the Basal Expression of Glutathione S-Transferases in Mouse Liver and to Their Induction by the Chemopreventive Synthetic Antioxidants, Butylated Hydroxyanisole and Ethoxyquin. *Biochem. Soc. Trans.* **2000**, *28* (2), 33–41. https://doi.org/10.1042/bst0280033.

(54) Yueh, M.-F.; Tukey, R. H. Nrf2-Keap1 Signaling Pathway Regulates Human UGT1A1 Expression in Vitro and in Transgenic UGT1 Mice *. *J. Biol. Chem.* **2007**, *282* (12), 8749–8758. https://doi.org/10.1074/jbc.M610790200.
(55) Gao, B.; Doan, A.; Hybertson, B. M. The Clinical Potential of Influencing Nrf2 Signaling in Degenerative and Immunological Disorders. *Clin. Pharmacol. Adv. Appl.* **2014**, *6*, 19–34. https://doi.org/10.2147/CPAA.S35078.
(56) Wu, K. C.; Cui, J. Y.; Klaassen, C. D. Beneficial Role of Nrf2 in Regulating NADPH Generation and Consumption. *Toxicol. Sci.* **2011**, *123* (2), 590–600. https://doi.org/10.1093/toxsci/kfr183.
(57) Lau, A.; Villeneuve, N. F.; Sun, Z.; Wong, P. K.; Zhang, D. D. Dual Roles of Nrf2 in Cancer. *Pharmacol. Res.* **2008**, *58* (5), 262–270. https://doi.org/10.1016/j.phrs.2008.09.003.
(58) Sporn, M. B.; Liby, K. T. NRF2 and Cancer: The Good, the Bad and the Importance of Context. *Nat. Rev. Cancer* **2012**, *12* (8), 564–571. https://doi.org/10.1038/nrc3278.
(59) Gupta, P.; Choudhury, S.; Ghosh, S.; Mukherjee, S.; Chowdhury, O.; Sain, A.; Chattopadhyay, S. Dietary Pomegranate Supplement Alleviates Murine Pancreatitis by Modulating Nrf2-P21 Interaction and Controlling Apoptosis to Survival Switch. *J. Nutr. Biochem.* **2019**, *66*, 17–28. https://doi.org/10.1016/j.jnutbio.2018.12.009.
(60) Hybertson, B. M.; Gao, B.; Bose, S.; McCord, J. M. Phytochemical Combination PB125 Activates the Nrf2 Pathway and Induces Cellular Protection against Oxidative Injury. *Antioxidants* **2019**, *8* (5), 119. https://doi.org/10.3390/antiox8050119.
(61) Sahin, N.; Akdemir, F.; Orhan, C.; Aslan, A.; Agca, C. A.; Gencoglu, H.; Ulas, M.; Tuzcu, M.; Viyaja, J.; Komorowskı, J. R.; Sahin, K. A Novel Nutritional Supplement Containing Chromium Picolinate, Phosphatidylserine, Docosahexaenoic Acid, and Boron Activates the Antioxidant Pathway Nrf2/HO-1 and Protects the Brain against Oxidative Stress in High-Fat-Fed Rats. *Nutr. Neurosci.* **2012**, *15* (5), 42–47. https://doi.org/10.1179/1476830512Y.0000000018.
(62) Zhang, G.; Wang, W.; Kang, Y.; Xue, Y.; Yang, H.; Zhou, C.; Shi, G. Chronic Testosterone Propionate Supplement Could Activated the Nrf2-ARE Pathway in the Brain and Ameliorated the Behaviors of Aged Rats. *Behav. Brain Res.* **2013**, *252*, 388–395. https://doi.org/10.1016/j.bbr.2013.05.063.
(63) Hybertson, B. M.; Gao, B.; Bose, S. K.; McCord, J. M. Oxidative Stress in Health and Disease: The Therapeutic Potential of Nrf2 Activation. *Mol. Aspects Med.* **2011**, *32* (4), 234–246. https://doi.org/10.1016/j.mam.2011.10.006.
(64) Lai, T.-H.; Shieh, J.-M.; Tsou, C.-J.; Wu, W.-B. Gold Nanoparticles Induce Heme Oxygenase-1 Expression through Nrf2 Activation and Bach1 Export in Human Vascular Endothelial Cells. *Int. J. Nanomedicine* **2015**, *10*, 5925–5939. https://doi.org/10.2147/IJN.S88514.
(65) Fuse, Y.; Endo, Y.; Araoi, S.; Daitoku, H.; Suzuki, H.; Kato, M.; Kobayashi, M. The Possible Repositioning of an Oral Anti-Arthritic Drug, Auranofin, for Nrf2-Activating Therapy: The Demonstration of Nrf2-Dependent Anti-Oxidative Action Using a Zebrafish Model. *Free Radic. Biol. Med.* **2018**, *115*, 405–411. https://doi.org/10.1016/j.freeradbiomed.2017.12.022.
(66) Tsoli, M.; Kuhn, H.; Brandau, W.; Esche, H.; Schmid, G. Cellular Uptake and Toxicity of Au55 Clusters. *Small* **2005**, *1* (8–9), 841–844. https://doi.org/10.1002/smll.200500104.

(67) Pan, Y.; Leifert, A.; Ruau, D.; Neuss, S.; Bornemann, J.; Schmid, G.; Brandau, W.; Simon, U.; Jahnen-Dechent, W. Gold Nanoparticles of Diameter 1.4 Nm Trigger Necrosis by Oxidative Stress and Mitochondrial Damage. *Small* **2009**, *5* (18), 2067–2076. https://doi.org/10.1002/smll.200900466.
(68) Senut, M.-C.; Zhang, Y.; Liu, F.; Sen, A.; Ruden, D. M.; Mao, G. Size-Dependent Toxicity of Gold Nanoparticles on Human Embryonic Stem Cells and Their Neural Derivatives. *Small Weinh. Bergstr. Ger.* **2016**, *12* (5), 631–646. https://doi.org/10.1002/smll.201502346.
(69) Sanchez-Cano, C.; Carril, M. Recent Developments in the Design of Non-Biofouling Coatings for Nanoparticles and Surfaces. *Int. J. Mol. Sci.* **2020**, *21* (3), 1007. https://doi.org/10.3390/ijms21031007.
(70) Ke, P. C.; Lin, S.; Parak, W. J.; Davis, T. P.; Caruso, F. A Decade of the Protein Corona. *ACS Nano* **2017**, *11* (12), 11773–11776. https://doi.org/10.1021/acsnano.7b08008.
(71) Corbo, C.; Molinaro, R.; Parodi, A.; Toledano Furman, N. E.; Salvatore, F.; Tasciotti, E. The Impact of Nanoparticle Protein Corona on Cytotoxicity, Immunotoxicity and Target Drug Delivery. *Nanomed.* **2015**, *11* (1), 81–100. https://doi.org/10.2217/nnm.15.188.
(72) Walkey, C. D.; Chan, W. C. W. Understanding and Controlling the Interaction of Nanomaterials with Proteins in a Physiological Environment. *Chem. Soc. Rev.* **2012**, *41* (7), 2780–2799. https://doi.org/10.1039/C1CS15233E.
(73) Oh, J. Y.; Kim, H. S.; Palanikumar, L.; Go, E. M.; Jana, B.; Park, S. A.; Kim, H. Y.; Kim, K.; Seo, J. K.; Kwak, S. K.; Kim, C.; Kang, S.; Ryu, J.-H. Cloaking Nanoparticles with Protein Corona Shield for Targeted Drug Delivery. *Nat. Commun.* **2018**, *9* (1), 4548. https://doi.org/10.1038/s41467-018-06979-4.
(74) Carrillo-Carrion, C.; Carril, M.; Parak, W. J. Techniques for the Experimental Investigation of the Protein Corona. *Curr. Opin. Biotechnol.* **2017**, *46*, 106–113. https://doi.org/10.1016/j.copbio.2017.02.009.
(75) Silvio, D. D.; Rigby, N.; Bajka, B.; Mayes, A.; Mackie, A.; Bombelli, F. B. Technical Tip: High-Resolution Isolation of Nanoparticle–Protein Corona Complexes from Physiological Fluids. *Nanoscale* **2015**, *7* (28), 11980–11990. https://doi.org/10.1039/C5NR02618K.
(76) Docter, D.; Distler, U.; Storck, W.; Kuharev, J.; Wünsch, D.; Hahlbrock, A.; Knauer, S. K.; Tenzer, S.; Stauber, R. H. Quantitative Profiling of the Protein Coronas That Form around Nanoparticles. *Nat. Protoc.* **2014**, *9* (9), 2030–2044. https://doi.org/10.1038/nprot.2014.139.
(77) Galmarini, S.; Hanusch, U.; Giraud, M.; Cayla, N.; Chiappe, D.; von Moos, N.; Hofmann, H.; Maurizi, L. Beyond Unpredictability: The Importance of Reproducibility in Understanding the Protein Corona of Nanoparticles. *Bioconjug. Chem.* **2018**, *29* (10), 3385–3393. https://doi.org/10.1021/acs.bioconjchem.8b00554.
(78) Walkey, C. D.; Olsen, J. B.; Song, F.; Liu, R.; Guo, H.; Olsen, D. W. H.; Cohen, Y.; Emili, A.; Chan, W. C. W. Protein Corona Fingerprinting Predicts the Cellular Interaction of Gold and Silver Nanoparticles. *ACS Nano* **2014**, *8* (3), 2439–2455. https://doi.org/10.1021/nn406018q.
(79) Wiśniewski, J. R.; Zougman, A.; Nagaraj, N.; Mann, M. Universal Sample Preparation Method for Proteome Analysis. *Nat. Methods* **2009**, *6* (5), 359–362. https://doi.org/10.1038/nmeth.1322.